Form Approved
OMB No 0704-0188

1. AGENCY USE ONLY (Leave blank)	2. REPORT DATE	3. REPORT TYPE AND DATES COVERED
	April 14, 1994	Final, Sept. 30, 1991 - Dec. 31, 1993

4. TITLE AND SUBTITLE

Domain Processes in Ferroelectric Ceramics

5. FUNDING NUMBERS

G AFOSR-91-0433

6. AUTHOR(S)

Wenwu Cao and L.E. Cross

7. PERFORMING ORGANIZATION NAME(S) AND ADDRESS(ES)

The Pennsylvania State University
110 Technology Center Bldg.
University Park, PA 16802

8. PERFORMING ORGANIZATION REPORT NUMBER

AFOSR-TR- 94 0308
N/A

9. SPONSORING/MONITORING AGENCY NAME(S) AND ADDRESS(ES)

Air Force Office of Scientific Research
Building 410
Bolling AFB DC 20332-6448

10. SPONSORING/MONITORING AGENCY REPORT NUMBER

11. SUPPLEMENTARY NOTES

12a. DISTRIBUTION/AVAILABILITY STATEMENT

Available to public upon request.

Approved for public release;
distribution unlimited.

12b. DISTRIBUTION CODE

13. ABSTRACT (Maximum 200 words)

This report outlines the progress achieved during a two year effort sponsored by the AFOSR on the theoretical study of domain and domain wall formation in ferroelectrics. Understanding on domain formation and domain dynamicsin ferroelectrics are crucial for developing better functional ceramic materials for transducers and actuators. A continuum model has been developed to describe the polarization profile in ferroelectrics, which takes into account both nonlinear and nonlocal nature of the ferroelectric system. The theory can give rise to twin and twin band solutions under proper boundary conditions. A theoretical model is also developed for the morphotropic phase boundary in PZT system, which provides a new interpretation on the phase coexistence in a complete solid solution system. According to the new definition, the width of the coexistence region is inversely proportional to the volume of the coherent region, such as the particle size for a fine grain system. Theoretical interpretation is provided to the electron interference pattern across a ferroelectric domain wall in holographic electron microscopy, a newly developed technique with much higher magnification than the conventional TEM. The relationship between microscopic lattice dynamics and the continuum theory is also established.

14. SUBJECT TERMS	15. NUMBER OF PAGES
Ferroelectric domains, domain walls, continuum theory, PZT, defect dopants, holographic electron microscopy, morphotropic phase boundary	16. PRICE CODE

17. SECURITY CLASSIFICATION OF REPORT	18. SECURITY CLASSIFICATION OF THIS PAGE	19. SECURITY CLASSIFICATION OF ABSTRACT	20. LIMITATION OF ABSTRACT
unclassified	unclassified	unclassified	UL

PENNSTATE

DOMAIN PROCESSES IN FERROELECTRIC CERAMICS

TECHNICAL REPORT FOR THE PERIOD OF
October 1, 1992 to December 31, 1993
by

L. E. Cross
Evan Pugh Professor of Electrical Engineering

Wenwu Cao
Associate Professor of Materials

AIR FORCE OFFICE OF SCIENTIFIC RESEARCH
Grant No AFOSR-91-0433

THE INTERCOLLEGE MATERIALS RESEARCH LABORATORY
UNIVERSITY PARK, PA

TABLE OF CONTENTS

I. INTRODUCTION

This is the final progress report for this two year program sponsored by the Air Force Office of Scientific Research on "Domain Processes in Ferroelectric Ceramics". As an issue which has both scientific and technical importance, domain process in ferroelectric ceramics has gain more and more attention in recent years, especially in the area of material development for transducers and smart structures. People are eager to know the mechanism of domain formation and domain dynamics in order to better process and engineer the required materials to achieve desired physical properties. This two year research has set a solid foundation to build upon for future studies aimed toward more thorough understanding of domain formation and domain dynamics.

As a continuation of the first year's effort (Appendix 5) we have made substantial new progress in the second year as described in this report. Due to the complexity of the problem and limited resources, we have focused on a few key issues emphasizing the basic theoretical development. The technical progress for the second year is outlined in each of the following sections, and the details can be found in the four appendices A1-A4. The technical report for the first year is attached as Appendix 5 for reference.

Section II describes the theory development. The key issue is the nonlocal coupling of the polarization vector. This nonlocal coupling is taken into account through a set of polarization gradient coefficients in the energy expansion, which eventually enter the equilibrium conditions in the Euler's equation. These gradient coefficients are proven to directly couple to the dispersion surface of the soft mode. In terms of the microscopic picture, the gradient energy is the mean field representation of the inter-site coupling of electric dipoles. The nonlocal coupling strength determines the domain wall width and the coherent length in domain dynamics. In Section III we report a study on the feasibility of using electron holography to ascertain the domain profiles, and try to extract the polarization gradient coefficients from the electron interference pattern. It is our belief that this direction is worth more effort in the future. Section IV states some combined experimental and theoretical effort trying to identify and understand more complicated microdomain structures and trying to find out the intrinsic mechanism behind the modulated nanoscale structures in doped ferroelectrics. Section VI highlights the current development and future plans which are generated through this project, and are still carrying on the momentum. Computer simulation on the domain dynamics is beginning to take off and we believe the dielectric dispersion in the domain dynamics will be understood through this study.

Many results were produced in this relatively short period of time and we hope the seeds planted here will flourish in the near future.

II. DOMAIN WALL PROFILE, POLARIZATION GRADIENTS, AND THE DISPERSION SURFACE OF SOFT MODE

Domain walls in ferroelectrics are the boundaries of different variants in the low temperature ferroelectric phase, which are generated during the paraelectric-ferroelectric phase transition. Due to the long range nature of the electric and elastic interactions, nonlocal coupling of the electric dipoles is very strong, and this nonlocal coupling determines the width of the domain walls. The formation of a spontaneous polarization can be well characterized by a Landau-Devonshire type theory[1]. Ferroelectric systems are also strongly nonlinear by including the nonlocal coupling in the free energy expansion in terms of polarization gradients, one can derive soliton-like solutions for the domain walls[A1]. These solutions reflect an intrinsic mechanism for the formation of domain walls without interface defects. It can be shown that these domain states have higher energy than single domain sate, however, they can be stabilized through twinband cross pining and/or by elastic or electric boundary conditions. The formulation described in Appendix A1 has included the elastic coupling as well as the nonlinearity and nonlocal coupling. One of the most important solutions is the polarization profile for a 90° domain wall. The spontaneous polarization is strongly coupled to the elastic strain in a 90° domain wall, therefore, is directly responsible for large portion of the field induced piezoelectric effect in ferroelectric ceramics.

Following the procedure described in A1, one can derive the temperature dependence of the domain profile for a tetragonal ferroelectric. As shown in Fig. 3 of Appendix A1, with the decrease of temperature, the magnitude of the spontaneous polarization increases but the domain wall thickness decreases, The changing rate for both the spontaneous polarization and the domain wall thickness are most noticeable near the transition temperature, both quantities eventually become insensitive to temperature for temperature much below Tc. Fig. 4 of Appendix A1 depicts the influence of the six order nonlinearity parameter. It affects very strongly on the symmetrical part of the polarization vector, which defines the local structural distortion inside the domain wall , but the influence on the antisymmetric part of the polarization is weak.

The most influential parameters for the domain wall thickness are the polarization gradient coefficients which reflect the strength of nonlocal coupling. This effect is illustrated in Fig. 2 of Appendix A1. In general, stronger nonlocal coupling will have broader domain wall. This is conceivable since the domain wall is actually a spatial transition region between two coherently distorted structures, it would be easier to transform from one domain state to the other when the nonlocal coupling is weak.

Using the formulism in Appendix A1 all the physical quantities associated with the ferroelectric domain walls can be calculated. However, the expansion coefficients in the free

energy [Eqs. (1-3) of Appendix A1] must be determined experimentally. The elastic, dielectric and electrostrictive coefficients can be directly measured and are readily available for many materials. The difficulty is the determination of the polarization gradient coefficients, which many researches only estimate through some hand waving arguments. It is shown in Appendix A2 that these gradient coefficients can be directly linked to the microscopic quantities and, in principle, can be also measured directly. A simplified rigid ion model has been developed for a perovskite system as described in Appendix A2. Since the polarization which is the density of electric dipoles can be directly related to the relative displacement vector of positive and negative charge centers, the gradient coefficients are actually directly related to the dispersion surface of the corresponding soft mode for the ferroelectric transition. Therefore, through inelastic neutron scattering experiments, one may be able to derive these polarization gradient coefficients. This work draws a clear link between the macroscopic Landau formulism and the fundament microscopic lattice dynamics. Although the problem has been cleared conceptually, in reality, it is far from completed since the required neutron experiments are very difficult to perform due to the high temperature involved. In several cases, the soft mode can be over damped which makes it impossible to measure. A recently emerged technique Electron Holography offers a new direction in this regard, which is described in the following section.

III. ELECTRON HOLOGRAPHY AND THE OBSERVATION OF FERROELECTRIC DOMAIN WALLS

Electron holography utilizing the wave characteristics of electrons. Through a sharp emission tip, the emitted electron beam is largely coherent, or in phase. While passing through an electric field region, the electron wave will experience a phase shift. If the field is inhomogeneous, the interference pattern formed on the recording film will be twisted.[2,3] Assuming no compensation at the surface of the electrodes, a twin structure will form a spatial varying electric field with large field gradient in the domain wall region. This in principle will cause a twist of the interference pattern produced by the transmitted electrons. From the twisted interference pattern, domain wall thickness can be evaluated with appropriate data interpretation. A typical twisted interference pattern is shown in Fig. 4 of Appendix A3, which is produced by coherent electrons transmitting through a 90° domain wall in $BaTiO_3$.[3] This new technique opens up a different avenue to obtain the gradient coefficients in the continuum theory described in Appendix A1, since one can do back fitting using the experimental data and the theoretical derived polarization profiles. However, as pointed out in ref. [4] that the charge compensation at the surface of the ferroelectric is unavoidable, therefore, the internal field supposed to be produced by the spontaneous polarization is actually shielded, so that the interference pattern

twisting will not be seen in many cases. These twisted interference patterns can be seen only in some situations when the compensation time constant is very long, or momentarily with the disturbance of temperature.[4] More thorough theoretical understanding is still needed to perfect the interpretation of the electron interference patterns.

Some charged defects inside the sample can also produce disturbance to the interference pattern through the electric field surrounding these defects. Fig. 5 in Appendix A3 shows this situation. An interesting point is the interaction of these charged defects with domain walls, it appears that they are attracted to the domain wall region. This observation provides an important evidence for the defect pinning to the domain walls, which gives us a possible explanation of why a few percent of aliovalent doping could change the physical properties of piezoelectric ceramic PZT so drastically[A3]. Many potential applications of this new technique await for further exploration.

IV. MICROSTRUCTURAL MODULATIONS IN PLT

In domain dynamics, the inertia associated with domain wall motion is quite large since the whole domain has to be moved in the perpendicular direction to the domain wall motion. It is conceivable that the domain wall motion will become easier when the domain size becomes smaller. Small domains may be achieved by aliovalent doping since the charged dopants have strong interaction with domain walls, hence will affect the domain formation. Smaller domain size makes it easier to switch and produces relatively larger dielectric response. Appendix A4 reports a study on Lanthanum doped lead titanate which produces a spectrum from pure ferroelectric to relaxor ferroelectric. As shown in Fig. 3 of Appendix A4, the domain structure changes from regular large size at 1% lanthanum doping to an ill-defined mirostructural modulation at 25% doping. The strongly first order ferroelectric phase transition in $PbTiO_3$ is also gradually changed to a nearly second order transition. The emerge of microdomain-like structures within a well defined domain during the increase of lanthanum doping provides a key for the understanding of dopant driven transition from a conventional ferroelectric to a relaxor ferroelectric. The domain signature gives us a direct way to distinguish between different types of ferroelectrics, the dielectric and piezoelectric performance of ferroelectric materials are also directly coupled to the domain structures.

V. PAPERS PRESENTED AT NATIONAL AND INTERNATIONAL MEETINGS

A: *INVITED TALKS*

L. E. Cross "Piezoelectric Sensors and Actuators for Smart Materials" Drexel University, Oct. 20-21, 1992.

L. E. Cross "Relaxor Ferroelectrics" Thgird International Ceramic Science and Technology Congress, Am. Ceram. Soc., San Francisco, Nov. 1-4, 1992.

L. E. Cross " Relaxor Ferroelectrics: Self Assembling Self Limiting Nanocomposites" Materials Research Society Medal/Award Lecture, Boston, Dec. 1-4, 1992.

L. E. Cross "Ferroelectric Materials and Devices: Current Issues and Future Prospects" Materials Research Soc. (Spring Mtg), San Francisco, April 12-16, 1993.

L. E. Cross "Micromechanical (MEMS) Systems bored on ferroelectric films" Am. Ceram. Soc. 95th Annual Mtg, Cincinnati, April 18-22, 1993.

L. E. Cross "Relaxor Ferroelectrics: An Overview" IMF8, Gaithersburg, Aug. 8-13, 1993.

L. E. Cross "Electronic Ceramics: New Actuators and Transducers" 1st Okmaga Symposium, Ikebukuro Tokyo, Aug. 29, 1993.

L. E. Cross "Relaxor Ferroelectrics: Useful Electronic Nanocomposites", IUMRS -ICAM 1993, Tokyo Japan, Aug. 31-Sep. 4, 1993.

L. E. Cross "Recent Development in Piezoelectric and Electrostrictive Sensors and Actuators" 1993 Pac Rim Mtg, Am. Ceram. Soc., Nov. 7- 10, 1993.

Wenwu Cao, "The Importance of Conventional and Holographic Electron Microscopy in the Fundamental Understanding of Ferroelectrics", The Second Williamsburg Workshop on Fundamental Experiments in Ferroelectrics (MIT/ONR), Williamsburg, Virginia, Feb. 1993.

B. CONTRIBUTED PAPERS

Wenwu Cao, "Theoretical Study on Domain Walls in $BaTiO_3$ " American Physical Society March Meeting, Seattle, Washington, 1993.

Wenwu Cao, "Nonlinear and Nonlocal Continuum Theory on Domain Walls in Ferroelectrics" IMF8, Rockville, Verginia, August, 1993.

G. A. Rosseetti, Jr., C. A. Randall and Wenwu Cao, "Microstructural Characteristics of Perovskite Ferroelectrics with diffuse Phase Transitions" IMF8, Rockville, Verginia, August, 1993.

VI. PROGRAMS IN PROGRESS

Although the current two years contract has come to a conclusion, the effort initiated by this Air Force grant has planted a seed for the future study of domain processes in ferroelectrics. The understanding on this subject is crucial in the development of functional ceramics. One of the natural extensions of this work is to study domain dynamics. According to our analyses, the problem may be simplified to a two-dimensional electric dipole problem with inter-site coupling. Therefore, molecular dynamics methods can be used. We are currently developing a computer program based on the formulation described in Appendix A1 and adding an alternating electric field. At the beginning stage, only one twin will be calculated, and later we plan to extend the calculation to multidomain configurations. The primary focus is on the 90° twin for which the elastic strain is directly coupled to the domain wall motion. It is anticipated that this calculation can shed light on the extrinsic contributions to the dielectric, piezoelectric and electrostrictive effects in ferroelectric ceramics.

We also plan to carry out more experimental works using electron holography technique, which not only helps to develop a powerful new technique for the study of domain ferroelectrics, but also can push forward the theoretical study on domain walls as well as understanding the interaction of domain walls and aliovalent dopants.

Many ambiguous points were cleared through this study, such as the morphotropic phase boundary in PZT, the development of microdomain structures through aliovalent doping, and the relationship between the macroscopic Landau theory and the microscopic lattice dynamics. A new technique for direct observation of the domain wall profile is analyzed and some theoretical ground works are set for the proper interpretation of electron interference patterns generated by coherent electron going through ferroelectric twins.

Many problems still exist in the domain studies, and it is our belief that the understanding of these domain processes not only will enhance our knowledge about this fascinating material structure, but also can provide firm theoretical background for the future development of better functional ceramics.

REFERENCES

[1]. M. J. Haun, E. Furman, S. J. Jang and L. E. Cross, Ferroelectrics, **99**, 13 (1989).

[2]. see more details about the technique in a review article by A. Tonomura, Rev., Mod. Phys., **59**, 639 (1987).

[3]. X. Zhang, T. Hashimoto, and D. C. Joy, Appl. Phys. Lett. **60**, 784 (1992).

[4]. W. Cao and C. A. Randall, Solid State Comm., **86**, 435 (1993).

Ferroelectrics, in press (1994).

A1

NONLINEAR AND NONLOCAL CONTINUUM THEORY ON DOMAIN WALLS IN FERROELECTRICS

WENWU CAO AND L. E. CROSS
Materials Research Laboratory, The Pennsylvania State University,
University Park, PA 16802

Abstract The domain structures in ferroelectrics can be described by a Landau-Ginzburg type theory with the twin and twin band (domain) structures being nonlinear and nonlocal excitations of the ferroelectric phase. The polarization gradients in the theory reflect the degree of nonlocal coupling along different crystallographic orientations. These gradient parameters can be obtained either from the dispersion surface of the soft mode or through fitting the polarization profile measured by the holographic electron microscopy.

INTRODUCTION

The understanding of domain structures is essential for the design and applications of ferroelectrics. It has been long recognized that the piezoelectric and dielectric properties of ferroelectric ceramics are mainly determined by the behavior of domain structures. The formation of domains in ferroelectrics is due to the existence of milti-variants in the ferroelectric phase. Atomic coherency is usually maintained across the domain boundaries, which make it possible to switch domain orientations from one to the other using external (either mechanical or electrical) fields. This switching gives rise to the so called extrinsic contributions to the materials properties. The formation of domain walls in ferroelectrics may be treated in terms of solitory wave excitations in a nonlinear and nonlocal system. Single kink-like and periodic solitory wave solutions for the twin and periodic domain structures can be derived using the continuum theory.[1-4] Since all the expansion coefficients in the Landau-Devonshire model can be expressed in terms of measurable macroscopic quantities, the continuum theory can give quantitative description of the domain wall properties, including the profile of polarization across the domain wall, domain wall width, energy stored in the muti-domain structure, and the stress build up at the domain wall region, once the polarization gradient coefficients are obtained.

THE MODEL

The Landau-Devonshire type phenomenological theory for ferroelectrics has been developed for the ferroelectric phase transition.[5,6,7] For a cubic system, such as perovskite ferroelectrics, the elastic Gibbs free energy can be expressed in the following form:

$$G = G_p + G_{el} + G_c \tag{1}$$

$$G_p = A (P_1^2 + P_2^2 + P_3^2) + B (P_1^4 + P_2^4 + P_3^4) + C (P_1^6 + P_2^6 + P_3^6) + D (P_1^2 P_2^2 + P_2^2 P_3^2 + P_1^2 P_3^2) + E (P_1^4 P_2^2 + P_1^2 P_2^4 + P_2^4 P_3^2 + P_2^2 P_3^4 + P_3^2 P_1^4 + P_1^2 P_3^4) + H P_1^2 P_2^2 P_3^2 \tag{2}$$

$$G_{el} = -\frac{s_{11}}{2} (X_{11}^2 + X_{22}^2 + X_{33}^2) - s_{12} (X_{11}X_{22} + X_{22}X_{33} + X_{11}X_{33}) - \frac{s_{44}}{2} (X_{12}^2 + X_{13}^2 + X_{23}^2) \tag{3}$$

$$G_c = Q_{11} (X_{11} P_1^2 + X_{22} P_2^2 + X_{33} P_3^2) + Q_{12} [X_{11} (P_2^2 + P_3^2) + X_{22} (P_1^2 + P_3^2) + X_{33} (P_1^2 + P_2^2)] + Q_{44} (X_{12} P_1 P_2 + X_{13} P_1 P_3 + X_{23} P_2 P_3) \tag{4}$$

where A, B, C, D, E, H are the linear and nonlinear dielectric constants, s_{ij} are the elastic compliance coefficients, Q_{ij} are the electrostriction constants, P_i and X_{ij} are the components of polarization and stress, respectively. All the coefficients are assumed to be independent of temperature except A which is a linearly function of T,

$$A = \alpha (T - T_0) \tag{5}$$

In a homogeneous system, a paraelectric-ferroelectric phase transition occurs at Tc. Under stress free condition, the phase transition temperature Tc and the spontaneous polarization P_c at the transition can be derived by minimizing Eq. (1),

$$T_c = T_0 + \frac{B^2}{4 C \alpha} \tag{6}$$

$$P_c^2 = \frac{-B}{2C}. \tag{7}$$

One of the low temperature ferroelectric phases is the tetragonal phase. There are six energetically degenerate variants in the tetragonal phase: $(\pm P_s, 0, 0)$, $(0, \pm P_s, 0)$ and $(0, 0, \pm P_s)$, where P_s is the spontaneous polarization given by

$$P_s = \sqrt{\frac{-B + \sqrt{B^2 - 3AC}}{3C}} \tag{8}$$

These energetically degenerate variants can coexist in the ferroelectric phase to form the twin structures. Electron microscopy reveals that the ionic coherency is maintained across domain walls, but domain walls are not atomically sharp. Domain wall width is determined by the nonlocal coupling strength of the ferroelectric system.

Since the nonlinearity has been included in the model [see Eqs. (1)-(4)], if we add the contributions of nonlocal coupling, then from soliton theory, we may expect solitory wave excitations in the ferroelectric phase. These excitations are in deed found and they represent the ferroelectric domain walls.

For a perovskite system, the symmetry of the high temperature phase is cubic, therefore, the Gibbs energy representing the nonlocal coupling can be written as follows:[2]

$$G_g = \frac{1}{2} g_{11} (P_{1,1}^2 + P_{2,2}^2 + P_{3,3}^2) + g_{12} (P_{1,1} P_{2,2} + P_{1,1} P_{3,3} + P_{2,2} P_{3,3}) + \frac{1}{2} g_{44} [(P_{1,2} + P_{2,1})^2 + (P_{1,3} + P_{3,1})^2 + (P_{2,3} + P_{3,2})^2] \quad (9)$$

here the indices after the comma represent derivatives with respect to space variable along that axis. Upon the minimization of the total free energy of the system Eqs. (1) and (9), one can obtain the solutions for the domain walls.[2]

90° DOMAIN WALLS

There are two types of domain walls in the tetragonal ferroelectrics. One is the 180° domain wall which divides a twin domain with identical strain but opposite polarization, and the other is the 90° domain wall which divides two domains whose polarization and spontaneous strain are nearly 90° from each other. Solutions for the 180° domain walls can be easily obtained since the problem is one-dimensional.[2] Here we only solve the problem of 90° domain walls for which the problem can be rendered to quasi-one-dimensional.

From transmission electron microscopy studies, domain walls tend to broaden or bent near the surface, however, inside the sample they have well defined wall-like

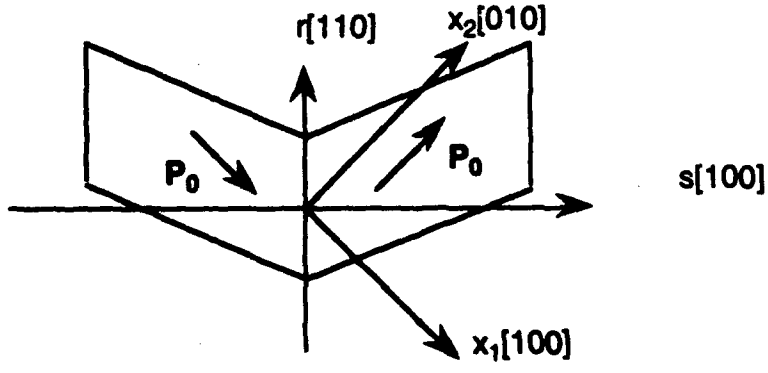

FIGURE 1. A tetragonal twin structure and the coordinate system used in this paper.

structure with translational symmetry parallel to the wall plane. Therefore, while dealing with a <110>-type domain walls in tetragonal ferroelectrics we can rotate the x_1, x_2 coordinates about the x_3 coordinate by 45° so that the properties of the domain walls only depend on one space variable (s-coordinate as indicated in Fig. 1) only.

In the new coordinate system the equilibrium conditions are governed by the following equations:[2]

$$\frac{\partial}{\partial x_j}\left[\frac{\partial G}{\partial P_{i,j}}\right] - \frac{\partial G}{\partial P_i} = 0\,, \qquad (i,j = s, r, 3) \tag{10}$$

$$X_{ij,j} = 0, \qquad (i,j = s, r, 3) \tag{11}$$

and we also need the elastic compatibility relations

$$\varepsilon_{ikl}\,\varepsilon_{jmn}\,x_{ln,km} = 0 \quad (i,j,k,l,m,n = s, r, 3) \tag{12}$$

to insure the elastic continuity since in our model the domain walls are intrinsic excitations, no defects are created in the domain wall region. x_{ln} is the component of elastic strain tensor and ε_{ikl} is the Levi-Civita density.

Eqs (11) and (12) has three nontrivial solutions:

$$X_{r3} = 0 \tag{13}$$

$$X_{rr} = \frac{1}{2\,(s_{11}s_{ss} - s_{12}^2)}\{[\,2s_{12}Q_{12} - s_{11}(Q_{11}+Q_{12})]P_0^2 - [\,2s_{12}Q_{12} - s_{11}(Q_{11}+Q_{12}-Q_{44})]P_s^2 - [2s_{12}Q_{12} - s_{11}(Q_{11}+Q_{12}+Q_{44})]P_r^2\} \tag{14}$$

$$X_{33} = \frac{1}{2(s_{11}s_{ss} - s_{12}^2)}\{[s_{12}(Q_{11}+Q_{12}) - 2s_{ss}Q_{12}]P_0^2 - [\,s_{12}(Q_{11}+Q_{12}+Q_{44}) - 2s_{ss}Q_{12}]P_r^2 - [s_{12}(Q_{11}+Q_{12}-Q_{44}) - 2s_{ss}Q_{12}]\,P_s^2\} \tag{15}$$

where

$$s_{ss} = \frac{1}{2}\left(s_{11}+s_{12}+\frac{s_{44}}{2}\right).$$

It can be easily verified that the two stress components X_{rr} and X_{33} are nonzero only in the vicinity of the domain wall. These nonzero stress components near the domain wall region is the cause of the faster etching rate which makes the domain walls visible through chemical etching technique.

In order to see the general trend of the variation of polarization profile without specifying the coefficients to a particular system, we normalize the polarization and the space variable s into dimensionless forms by the following substitutions:

$$P_r = \sqrt{-\frac{B}{2C}}\; f_r = P_c\, f_r \qquad P_s = \sqrt{-\frac{B}{2C}}\; f_s = P_c\, f_s \tag{16a,b}$$

$$s = \gamma\,\xi, \qquad \gamma = \left(\frac{G_{ss}\,G_{rs}}{4\,A_c^2}\right)^{1/4} \tag{17a,b}$$

where

$$G_{ss}=\frac{1}{2}(g_{11}+g_{12}+2g_{44}), \qquad G_{rs}=\frac{1}{2}(g_{11}-g_{12}),$$

and define the dimensionless temperature as

$$\tau=\frac{T - T_0}{T_c - T_0} \tag{18}$$

then the equilibrium condition Eq. (10) can be written in the following form for a 90° twin structure,

$$a\, f_{s,\xi\xi}= \tau_s\, f_s+ b_s f_s^3+ c\, f_s f_r^2+ d f_s^5+ (8 - \frac{2}{3}d)\, f_s^3 f_r^2+ (4 - \frac{1}{3}d)\, f_s f_r^4 \tag{19}$$

$$\frac{1}{a} f_{r,\xi\xi}= \tau_r\, f_r+ b_r f_r^3+ c\, f_r f_s^2 + d f_r^5+ (8 - \frac{2}{3}d)\, f_r^3 f_s^2+ (4 - \frac{1}{3}d)\, f_r f_s^4 \tag{20}$$

where the coefficients are given by

$$a=\sqrt{\frac{G_{ss}}{G_{rs}}} \tag{21}$$

$$\tau_s=\tau-\frac{(1+\sqrt{1-\frac{3}{4}\tau})}{3(s_{11}s_{ss}-s_{12}^2)B}\{(Q_{11}+Q_{12}-Q_{44})[2s_{12}Q_{12}-s_{11}(Q_{11}+Q_{12})] +2Q_{12}[s_{12}(Q_{11}+Q_{12})-2s_{ss}Q_{12}]\} \tag{22}$$

$$\tau_r=\tau\frac{(1+\sqrt{1-\frac{3}{4}\tau})}{3(s_{11}s_{ss}-s_{12}^2)B}\{(Q_{11}+Q_{12}+Q_{44})[2s_{12}Q_{12}-s_{11}(Q_{11}+Q_{12})] +2Q_{12}[s_{12}(Q_{11}+Q_{12})-2s_{ss}Q_{12}]\} \tag{23}$$

$$b_s= -2-\frac{D}{B}+\frac{1}{2B(s_{11}s_{ss}-s_{12}^2)}\{(Q_{11}+Q_{12}-Q_{44})[2s_{12}Q_{12}-s_{11}(Q_{11}+Q_{12}-Q_{44})] +2Q_{12}[s_{12}(Q_{11}+Q_{12}-Q_{44})-2s_{ss}Q_{12}]\} \tag{24}$$

$$b_r = -2-\frac{D}{B}+\frac{1}{2B(s_{11}s_{ss}-s_{12}^2)}\{(Q_{11}+Q_{12}+Q_{44})[2s_{12}Q_{12}-s_{11}(Q_{11}+Q_{12}+Q_{44})] +2Q_{12}[s_{12}(Q_{11}+Q_{12}+Q_{44})-2s_{ss}Q_{12}]\} \tag{25}$$

$$c = -6+\frac{D}{B}+\frac{1}{2B(s_{11}s_{ss}-s_{12}^2)}\{(Q_{11}+Q_{12}-Q_{44})[2s_{12}Q_{12}-s_{11}(Q_{11}+Q_{12}+Q_{44})] +2Q_{12}[s_{12}(Q_{11}+Q_{12}+Q_{44})-2s_{ss}Q_{12}]\} \tag{26}$$

$$d=\frac{3}{4}(1+\frac{E}{C}) \tag{27}$$

RESULTS AND DISCUSSIONS

Using the normalized equations, we can study the influence of different parameters to the polarization profile and obtain a conceptual understanding on the nature of the polarization variation in the domain wall region. Fig. 2 shows the variation of the polarization components with the parameter a across a 90° domain wall. One can see that the domain wall becomes wider as a increases. In real dimensions, because the scaling factor of the space variables, γ, is directly related to the product $G_{ss}*G_{rs}$ [see eq.(17)], domain wall becomes wider as the gradient coefficients become larger.

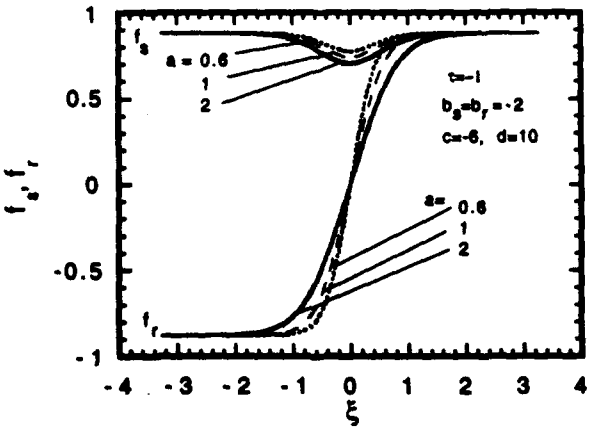

FIGURE 2. Variation of polarization components f_S and f_T induced by the change of parameter a across a 90° domain wall. The gradient parameter a determines the width of the domain wall.

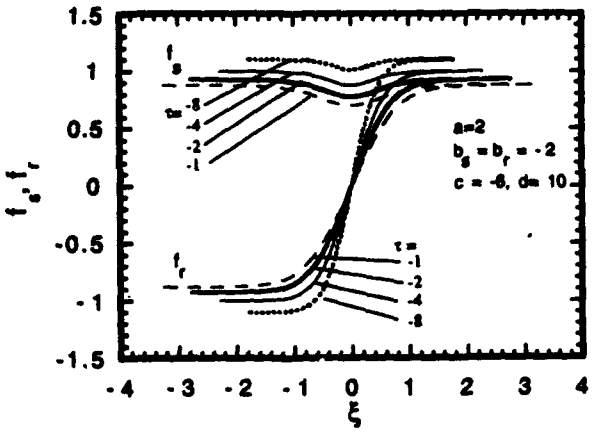

FIGURE 3. Variation of polarization components f_S and f_T with temperature τ across a 90° domain wall. The asymptotic values of the polarization components increase and the domain wall width decrease while lowering temperature.

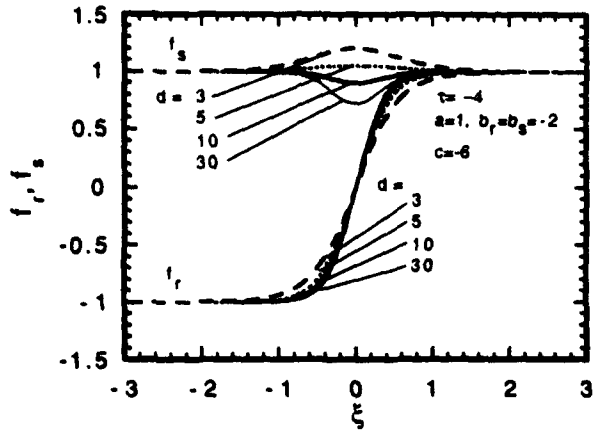

FIGURE 4. Variation of polarization components f_S and f_r induced by the change of parameter *d* across a 90° domain wall. The nonlinear parameter *d* influences the magnitude of the polarization variation in the domain wall region.

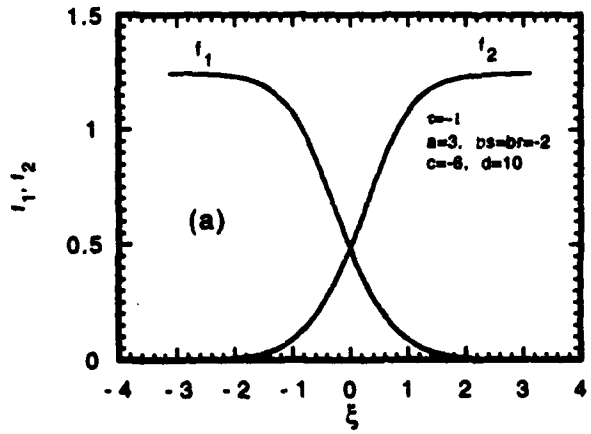

FIGURE 5. (a) Polarization components f_1 and f_2 across a 90° domain wall, and (b) Illustration of the variations of the polarization vector and the unite cell distortion across a 90° domain wall.

Fig. 3 shows the variation of the polarization with temperature τ. The asymptotic values of the magnitude of the polarization components increase and the domain wall thickness decreases as the temperature is lowered. The temperature dependence is strong near the transition and gradually becomes insensitive when the temperature is far below T_C. Fig. 4 shows the variation of the polarization components f_s and f_r induced by the change of parameter d. We can see that the magnitude of f_s is very sensitive to d while the domain wall thickness is relative insensitive to d. We can also calculate the polarization components f_1 and f_2 in the original coordinates. One example is given in Fig. 5 (a) for a set of chosen parameters. The corresponding unit cell distortion and the polarization variation across the domain wall are illustrated in Fig. 5(b). The polarization vector rotates gradually from one orientation into the other accompanied also by a change of the magnitude.

All properties of the domain walls can be quantitatively calculated using this model once the expansion coefficients are known. As we have mentioned above that the polarization gradient coefficients are most crucial for the study of domain walls, which may be derived from the measurements on the dispersion surface of the soft mode.[8,9] In general, inelastic neutron scattering to probe the soft mode may be difficult due to the relatively high transition temperature in many systems of interest and in some cases, the soft mode is over damped. An alternative way to obtain these coefficients would be to probe the polarization profile across the domain wall and then fitting the unknown coefficients using the differential equations (19) and (20). The recently emerged new technique, electron holography, may offer an option to this end.[10,11]

ACKNOWLEDGEMENTS

This research is sponsored by the Air Force Office of Scientific Research.

REFERENCES

1. V. A. Zhirnov, Zh. Eksp. Teor. Fiz. 35, 1175 (1958) [Sov. Phys. JETP 35, 822 (19590].
2. W. Cao and L. E. Cross, Phys. Rev. B 44, 5 (1991).
3. F. Falk, Z. Phys. B 51, 177 (1983).
4. G. R. Barsch and J. A. Krumhansl, Phys. Rev. Lett., 11, 1069 (1984).
5. A. F. Devonshire, Phil. Mag., 40, 1040 (1949); 42, 1065 (9151).
6. W. R. Bussem, L. E. Cross and A. K. Goswami, J. Amer. Ceram. Soc., 49, 33 (1966).
7. A. J, Bell and L. E. Cross, Ferroelectrics, 59 (1984).
8. W. Cao and G. R. Barsch, Phys. Rev. B 41, 4334 (1990).
9. K. Gesi, J. D. Axe, G. Shirane and A. Linz, Phys. Rev. B 5, 1933 (1972).
10. X. Zhang, T. Hashimoto and D. C. Joy, Appl. Phys. Lett. 60, 784 (1992).
11. W. Cao and C. A. Randall, Solid State Comm. 86, 435 (1993).

A2

Polarization Gradient Coefficients and the Dispersion Surface of the Soft Mode in Perovskite Ferroelectrics

Wenwu Cao

Materials Research Laboratory, The Pennsylvania State University, University Park, Pennsylvania 16802

Abstract

The gradient coefficients in the Landau-Ginzburg theory are crucial for quantitative description of domain walls in ferroelectrics. The magnitude of these gradient coefficients are a measure of nonlocal coupling strength of the polarization. In this paper, we intend to explain the physical meaning of these gradient coefficients in terms of lattice dynamics and give some relationships between these gradient coefficients and the dispersion surface of the soft mode. The implications for the study of over damped soft modes are also discussed.

PACS Numbers: 64.60.-i, 63.20.Dj, 64.90.+b

I. Introduction

Many ferroelectric materials have perovskite structure with a cubic symmetry in the paraelectric phase. The symmetry of the low temperature ferroelectric phase can be tetragonal, rhombohedral or orthorhombic. Ferroelectric phases usually have more than one variants and these variants may coherently coexist within the symmetry frame of the parent phase, forming the so called twin structures. It is shown that these twin structures can be well described by Landau-Ginzburg (LG) type models.[1,2] All the expansion coefficients in the Landau theory correspond to certain macroscopic physical quantities and can be obtained experimentally. However, the physical meaning of the gradient coefficients, which regulate the domain wall formation and control the domain wall width in the twin structures, still needs to be specified.

A paraelectric-ferroelectric phase transition is characterized by a softening of a transverse optic mode at the Brillouin zone center due to the cancelation of the long range Coulomb forces and the short range repulsive forces.[3] The soft mode is stabilized above the phase transition temperature by the anharmonic interactions whose strength weakens as the temperature decreases. Using mean field theory, one can still formally retain the terminology of normal modes if the "soft mode" frequency is assigned to be temperature dependent.

Close to the phase transition temperature, the dominant contribution in the lattice Hamitonian is from the soft mode. Therefore, one may simply study the soft mode behavior to characterize the phase transition near T_c. For an inhomogeneous system, the spatial variation of the order parameter must be considered. This is done by adding an energy term induced by the order parameter gradients. Because the inclusion of both nonlinear and nonlocal terms in the energy expansion, one may expect to obtain large amplitude soliton-like solutions which can describe the domain walls (the transition region between coherent twin structures).[4,5,6] The physical meaning of these gradient coefficients can be seen from the study of small amplitude oscillations for which the nonlocal coupling can be treated as perturbations.[6,7] We will show in

this paper how these polarization gradients can be derived from a simplified lattice dynamical model.

Since polarization is the density of dipoles per unit volume, it is proportional to the magnitude of the associated optical mode. As will be shown in the third section of this paper that the lattice potential for a given optical mode can be written in terms of the polarization vector. Therefore, the Landau-Ginzburg potential can be directly used in the lattice dynamical calculations in the small representation of the soft mode.

II. Gradient Coefficients and Dispersion Surface of the Soft Mode

From soft mode theory, the potential energy for a cubic system may be expanded in terms of the eigenvector of the soft mode[3]

$$G = \frac{\kappa}{2}(u_1^2 + u_2^2 + u_3^2) \qquad (1)$$

where κ is related to the temperature dependent soft mode frequency, $\kappa \propto (T-T_c)$, and u_i (i = 1,2,3) are the components of the eigenvector of the soft mode. For the ferroelectric phase transition **u** is a relative displacement field.

If **u** is inhomogeneous, we must include the gradient energy in the energy expansion. For cubic symmetry the gradient energy may be written as follows,

$$G_g = \frac{\delta_{11}}{2}(u_{1,1}^2 + u_{2,2}^2 + u_{3,3}^2) + \delta_{12}(u_{1,1}u_{2,2} + u_{1,1}u_{3,3} + u_{2,2}u_{3,3}) + \frac{\delta_{44}}{2}((u_{1,2}+u_{2,1})^2 + (u_{1,3}+u_{3,1})^2 + (u_{2,3}+u_{3,2})^2) \qquad (2)$$

Assuming the effective mass for the mode is M then the equations of motion become

$$M\ddot{u}_1 + \kappa u_1 - \delta_{11}u_{1,11} - \delta_{12}(u_{2,21} + u_{3,31}) - \delta_{44}(u_{1,22} + u_{2,12} + u_{1,33} + u_{3,13}) = 0, \qquad (3a)$$

$$M\ddot{u}_2 + \kappa u_2 - \delta_{11}u_{2,22} - \delta_{12}(u_{1,12} + u_{3,32}) - \delta_{44}(u_{1,21} + u_{2,11} + u_{2,33} + u_{3,23}) = 0, \qquad (3b)$$

$$M\ddot{u}_3 + \kappa u_3 - \delta_{11}u_{3,33} - \delta_{12}(u_{1,13} + u_{2,23}) - \delta_{44}(u_{1,31} + u_{3,11} + u_{2,32} + u_{3,22}) = 0, \qquad (3c)$$

Eq.(3a-c) have plane wave solution of the form

$$\mathbf{u} = \mathbf{U}\exp[j(\omega t - \mathbf{k}\cdot\mathbf{x})] \qquad (4)$$

Substituting eq. (4) into eqs. (3a-c) gives the eigenvalue problem

$$M\omega^2 U = \tilde{D}(k)\, U \qquad (5)$$

where $\tilde{D}(k)$ is the dynamical matrix

$$\tilde{D}(k)=\begin{pmatrix} \kappa+\delta_{11}k_1^2+\delta_{44}(k_2^2+k_3^2) & \delta_{12}\, k_1\, k_2 & \delta_{12}\, k_1\, k_3 \\ \delta_{12}\, k_1\, k_2 & \kappa+\delta_{11}k_2^2+\delta_{44}(k_1^2+k_3^2) & \delta_{12}\, k_2\, k_3 \\ \delta_{12}\, k_1\, k_3 & \delta_{12}\, k_2\, k_3 & \kappa+\delta_{11}k_3^2+\delta_{44}(k_1^2+k_2^2) \end{pmatrix} \qquad (6)$$

If the depolarization field is included, the equations of motion (3a-c) will contain one more term representing this contribution, which will split the longitudinal and transverse optical modes.[8,9] The depolarization field is given by

$$\mathbf{E}(\mathbf{k}) = -\frac{(\mathbf{P}\cdot\mathbf{k})}{\varepsilon_0}\,\frac{\mathbf{k}}{k^2} \qquad (7)$$

The additional contribution is a linear function of the polarization vector **P** which is proportional to the relative displacement field **u**. Adding eq. (7) to the r.h.s. of eq. (3a-c) leads to the dynamical matrix for a given **k**. In what follows, we will treat three **k**-values in the three principle directions of the **k**-space.

A. $\mathbf{k} = [\,k, 0, 0]$.

Define $P_i = Z\, e\, u_i$, where Z is a constant which has a unit of inverse volume and e is the electron charge unit. The meanigng of Z will be clear from later derivations. For this **k** value, the dynamical matrix can be simplified to the following form

$$\tilde{D}(k)=\begin{pmatrix} \kappa+A+\delta_{11}k^2 & 0 & 0 \\ 0 & \kappa+\delta_{44}\, k^2 & 0 \\ 0 & 0 & \kappa+\delta_{44}\, k^2 \end{pmatrix} \qquad (8)$$

where A is a constant defined by

$$A = (1/\varepsilon_0)\,(Z\, e)^2 \qquad (9)$$

From Eq. (8) one can easily derive the dispersion relations for the longitudinal (ω_L) and transverse (ω_T) modes respectively:

$$\omega_L^2 = \frac{1}{M}(\kappa + A + \delta_{11} k^2) \qquad (10a)$$

$$\omega_T^2 = \frac{1}{M}(\kappa + \delta_{44} k^2) \qquad (10b)$$

B. $\mathbf{k} = \frac{k}{\sqrt{2}} [1, 1, 0]$

The electrostatic force from the depolarization field is now given by

$$\frac{Z e (P_1 + P_2)}{2 \varepsilon_0} [1,1, 0] = \frac{A (u_1 + u_2)}{2} [1, 1, 0] \qquad (11)$$

Therefore the dynamical matrix is

$$\tilde{D}(\mathbf{k}) = \begin{pmatrix} \kappa + A/2 + (\delta_{11}+\delta_{44}) k^2/2 & A/2 + \delta_{12} k^2 & 0 \\ A/2 + (\delta_{12}/2) k^2 & \kappa + A/2 + (\delta_{11}+\delta_{44}) k^2/2 & 0 \\ 0 & 0 & \kappa + \delta_{44} k^2 \end{pmatrix} \qquad (12)$$

and the dispersion relations are

$$\omega_L^2 = \frac{1}{M}[\kappa + A + \frac{1}{2}(\delta_{11} + \delta_{12} + \delta_{44}) k^2] \qquad (13a)$$

$$\omega_{T_1}^2 = \frac{1}{M}[\kappa + \frac{1}{2}(\delta_{11} - \delta_{12} + \delta_{44}) k^2] \qquad (13b)$$

$$\omega_{T_2}^2 = \frac{1}{M}[\kappa + \delta_{44} k^2] \qquad (13c)$$

Here the two transverse modes are not degenerate.

C. $\mathbf{k} = \frac{k}{\sqrt{3}} [1, 1, 1]$.

For this case the Coulomb force from the depolarization field is

$$\frac{Z e (P_1 + P_2 + P_3)}{3 \varepsilon_0} [1,1, 1] = \frac{A (u_1 + u_2 + u_3)}{3} [1, 1, 1] \qquad (14)$$

and the dynamical matrix becomes

$$\tilde{D}(k)=\begin{pmatrix} \kappa+A/3+(\delta_{11}/3+2\,\delta_{44}/3)\,k^2 & A/3+(\delta_{12}/3)\,k^2 & A/3+(\delta_{12}/3)\,k^2 \\ A/3+(\delta_{12}/3)\,k^2 & \kappa+A/3+(\delta_{11}/3+2\,\delta_{44}/3)\,k^2 & A/3+(\delta_{12}/3)\,k^2 \\ A/3+(\delta_{12}/3)\,k^2 & A/3+(\delta_{12}/3)\,k^2 & \kappa+A/3+(\delta_{11}/3+2\,\delta_{44}/3)\,k^2 \end{pmatrix} \quad (15)$$

The dispersion relations are therefore given by

$$\omega_L^2 = \frac{1}{M}\left[\kappa + A + \frac{1}{3}(\delta_{11}+2\,\delta_{12}+2\,\delta_{44})\,k^2\right] \quad (16a)$$

$$\omega_T^2 = \frac{1}{M}\left[\kappa + \frac{1}{3}(\delta_{11}-\delta_{12}+2\,\delta_{44})\,k^2\right] \quad (16b)$$

Note that the dispersion relations derived above are for the cubic phase near k=0 but not for the low temperature ferroelectric phase.

III. The Expansion Coefficients and Lattice Dynamics

Taking the limit $\mathbf{k} \rightarrow 0$ in the dispersion relations derived above, one finds that the coefficient κ / M becomes the soft transverse mode frequency square,

$$\lim_{\mathbf{k}\rightarrow 0} \quad \omega_T^2 = \kappa / M \quad (17)$$

The longitudinal mode will not become soft at $T = T_c$ because of the depolarization field contribution A,

$$\lim_{\mathbf{k}\rightarrow 0} \quad \omega_L^2 = \frac{1}{M}(\kappa + A) \quad (18)$$

The simplest model to calculate these coefficients in terms of microscopic quantities is to study the $\mathbf{k}=0$ mode for a biatomic system using rigid ion model, in which the soft mode represents the relative displacement field, the mass is the relative mass, and the polarization is equal to the ionic charge times the relative displacement then devided by the unit cell volume. However, in the perovskite structure there are three different types of ions, hence, a more realistic

model would be a three body system model. In what follows we will use a one dimensional rigid ion model for $BaTiO_3$ as an example to illustrate the relationship between the coefficients in Eq. (1) and the microscopic quantities.

According to the structural work of Shirane et al,[10] the soft optical mode in $BaTiO_3$ consists of the relative motion of Titanium, Barium and Oxygen (Fig. 1a). Because the center of mass and the center of charge for each type of ions coincide, we can effectively treat this system as a three-body system in the lattice dynamical calculations. For convenience the ion groups are labeled as follows (see Fig. 1b): Ba --- 1; Ti --- 2; and 3 O ---3.

The potential energy represents the k = 0 mode for this three-body system is

$$\Phi = \frac{\kappa_1}{2}(x_1 - x_2)^2 + \frac{\kappa_2}{2}(x_2 - x_3)^2 \qquad (19)$$

In order to derive the equations of motion one should also consider the Lorentz field, which leads to the following differential equations:

$$m_1 \ddot{x}_1 = -\kappa_1 (x_1 - x_2) + \frac{1}{3\varepsilon_o} q_1 P \qquad (20\,a)$$

$$m_2 \ddot{x}_2 = -\kappa_1 (x_2 - x_1) - \kappa_2 (x_2 - x_3) + \frac{1}{3\varepsilon_o} q_2 P \qquad (20\,b)$$

$$m_3 \ddot{x}_3 = -\kappa_2 (x_3 - x_2) + \frac{1}{3\varepsilon_o} q_3 P \qquad (20\,c)$$

$$q_1 + q_2 + q_3 = 0 \qquad (21)$$

$$P = (q_1 x_1 + q_2 x_2 + q_3 x_3) / a_o^3 \qquad (22)$$

where a_o is the lattice constant, q_1, q_2, q_3 are the charges of the three ion groups, P is the polarization.

For convenience let us introduce two new variables

$$u = x_1 - x_3; \quad v = x_2 - x_3.$$

Using eqs. (21) and (22), and the new variables *u* and *v* the equations of motion (20a-c) can be simplified to become

$$\ddot{u} = a\,u + b\,v \qquad (23a)$$

$$\ddot{v} = c\,u + d\,v \qquad (23b)$$

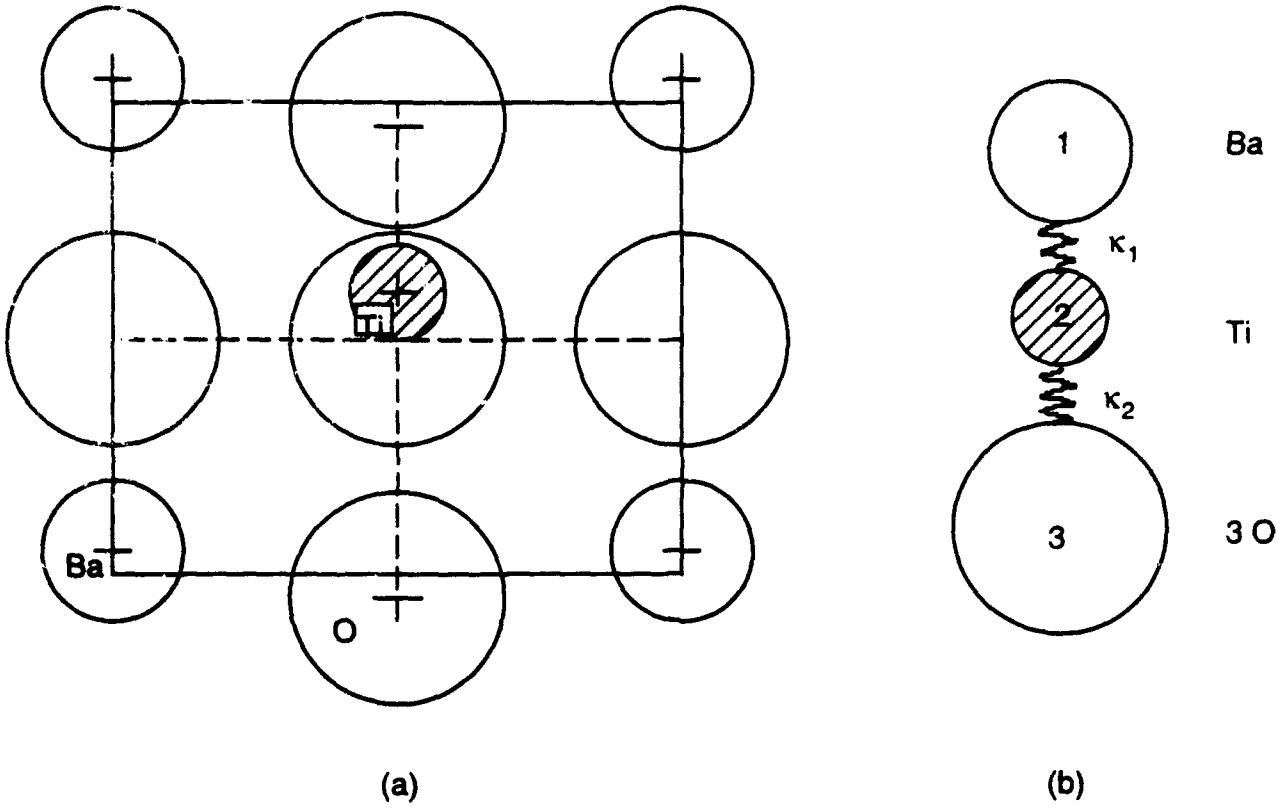

Figure 1. (a) Illustration of the ionic displacement in $BaTiO_3$ from ref. 10.
(b) One dimensional modal for the soft mode

where

$$a = -\frac{k_1}{m_1} + \frac{q_1}{3\varepsilon_o a_o^3}\left(\frac{q_1}{m_1} + \frac{q_1 + q_2}{m_3}\right)$$

$$b = -\left(\frac{k_2}{m_3} - \frac{k_1}{m_1}\right) + \frac{q_2}{3\varepsilon_o a_o^3}\left(\frac{q_1}{m_1} + \frac{q_1 + q_2}{m_3}\right)$$

$$c = \frac{k_1}{m_2} + \frac{q_1}{3\varepsilon_o a_o^3}\left(\frac{q_2}{m_2} + \frac{q_1 + q_2}{m_3}\right)$$

$$d = -\left(\frac{k_1 + k_2}{m_2} + \frac{k_2}{m_3}\right) + \frac{q_2}{3\varepsilon_o a_o^3}\left(\frac{q_2}{m_2} + \frac{q_1 + q_2}{m_3}\right)$$

Eqs (23a,b) have the harmonic oscillator solution

$$u = u_0 \exp(j\omega t) \qquad (24)$$

$$v = v_0 \exp(j\omega t) \qquad (25)$$

and the eigenfrequency ω is given by

$$\omega_{\pm}^2 = \frac{1}{2}\left[-a - d \pm \sqrt{(a+d)^2 - 4(ad - bc)}\right] \qquad (26)$$

In any given mode the relative displacement u and v are proportional to each other. For the coordinate system in Fig. 1, u and v always have the same sign. Assuming one of the modes, for example ω_-, becomes soft at lower temperatures due to the decrease of the coupling strength between different ions, then, their magnitudes have the following relationship:

$$v_0 = \frac{1}{2b}\left(d - a + \sqrt{(a+d)^2 - 4(ad - bc)}\right) u_0 \qquad (27)$$

From Eqs. (21) and (22) the polarization P is given by

$$P = (q_1 u + q_2 v)/a_o^3 = \left[q_1 + \frac{q_2}{2b}\left(d - a + \sqrt{(a+d)^2 - 4(ad - bc)}\right)\right] u/a_o^3 \qquad (28)$$

Therefore, in this mode

$$Ze = \left[q_1 + \frac{q_2}{2b}\left(d - a + \sqrt{(a+d)^2 - 4(ad - bc)}\right)\right]/a_o^3 \qquad (29)$$

The value of P can be obtained from pyroelectric measurements and u may be calculated from X-ray diffractions of the low and high temperature phases, hence, Ze can also be obtained experimentally.

Since v and P are linearly proportional to u, we could simplify the problem by constructing a new single variable potential $G = (\kappa/2)\, u^2$ which gives rise to the following equation of motion.

$$\begin{aligned} \ddot{u} &= a\,u + b\,v \\ &= \frac{1}{2}\left[-(a+d) - \sqrt{(a+d)^2 - 4(ad-bc)} \right] u \\ &= \frac{\kappa}{M}\, u \end{aligned} \qquad (30)$$

where κ has the dimension of force constant and M has the dimension of mass according to the definition of a, b, c and d. For a three dimensional system, the constructed potential which leads to Eq.(30) will have the same form as Eq. (1) according to symmetry. Because u is also proportional to the polarization P [eq. (28)], we may also write down the constructed potential in terms of the polarization vector P, which becomes the Landau potential for a ferroelectric system $G = (\alpha/2)\, P^2$, $\alpha = \kappa / (Z\, e)^2$.

For longitudinal vibrations, we have to add the depolarization field $(-P/\varepsilon_0)$ to the equation of motion Eq.(20 a -c), which will add a positive contribution to the eigenfrequency preventing it to become soft like the transverse mode. Formally, the relationship between ω_L and ω_T may be written as

$$\omega_L^2 = \omega_T^2 + \frac{A}{M} \qquad (30)$$

where A is a positive constant reflecting the contribution of the depolarization field.

IV. Summary and conclusions

It is shown that the polarization gradient coefficients in the Landau-Ginzburg theory can be directly related to the dispersion surface of the soft mode. Therefore, their physical meaning becomes apparent. The correspondence between the Landau theory and the lattice dynamic potential was illustrated through a simple one dimensional rigid ion model for $BaTiO_3$ at $\mathbf{k}=0$. Since the polarization and the relative displacement field have a linear relationship, the polarization gradient coefficients in the Landau-Ginzburg theory may be calculated from the measured dispersion curves near the soft mode. For cubic symmetry there are only three independent gradient coefficients, the dispersion anisotropy of the soft mode can be determined through

measurements along the three principal directions. These gradient coefficients in principle can be obtained through inelastic neutron scattering experiments. However, in many cases these dispersion curves are very difficult to measure because of the high transition temperature. To my knowledge, a complete set of the dispersion relations do not exist in the literatures for the known ferroelectric materials. One of the intentions of this paper is to re-emphasize the importance to measure these dispersion curves which can be used for the study of domain walls in ferroelectrics.

An interesting point should be also mentioned is the possibility of obtaining the dispersion surface of the soft mode through direct measurements on the domain wall profiles[11], because the gradient coefficients can be extracted from fitting the measured polarization profiles to the soliton-like solutions of nonlinear nonlocal continuous medium theory.[2,6] This could be very useful to study the dispersion surface of the over damped soft mode, such as in $BaTiO_3$, which can not be obtained through inelastic neutron scattering.

Acknowledgements

This research is sponsored by the Air Force Office of Scientific Researech.

Reference

1. V. A. Zhirnov, Zh. Eksp. Teor. Fiz. **35**, 1175 (1958) [Sov. Phys. JETP **35**, 822 (19590]
2. W. Cao and L. E. Cross, Phys. Rev. B **44**, 5 (1991).
3. W. Cochran, Advances in Phys., **9**, 387 (1960).
4. J. A. Krumhansl and J. R. Schrieffer, Phys. Rev. B **11**, 3535 (1975).
5. G. R. Barsch and J. A. Krumhansl, Phys. Rev. Lett., **11**, 1069 (1984).
6. W. Cao and G. R. Barsch, Phys. Rev. B **41**, 4334 (1990).
7. K. Gesi, J. D. Axe, G. Shirane and A. Linz, Phys. Rev. B **5**, 1933 (1972).

A3

Spatial Variations of Polarization in Ferroelectrics and Related Materials

C.A.Randall, G.A. Rossetti, Jr., and W. Cao
Materials Research Laboratory
The Pennsylvania State University
University Park, PA 16802

Abstract

Electron microscopy studies in lanthanum doped lead titanate reveals the evolution of a spatial modulation in the magnitude of the spontaneous polarization with the increase of the lanthanum dopant. On the incorporation of ~ 25 atom percent lanthanum, the conventional domain structure becomes ill-defined, and tweed microstructures are observed. The structural information can be associated with the change from normal ferroelectric to diffuse ferroelectric phase transition behavior. Different from twin structures, these modulated structures represent a new type of polarization variation existing within a single domain. Further understanding of the observed spatial variation in polarization requires structural analysis at the atomic scale. Holographic electron microscopy is proposed as a potential tool to study various polarization gradients in ferroelectric materials. Understanding the spatial variations in polarization is essential to more fully comprehend the extrinsic contributions to the elasto-dielectric properties in ferroelectrics.

Introduction

Mesoscopic structures within ferroelectrics and related materials have important consequences with respect to the macroscopic elasto-dielectric properties. These structures exist on a scale of a few tens to a few thousands of angstroms and include defect structures within the lattice as well as the polarization domain structures associated with the ferroic phase transition. In general, there are two contributions to the elasto-dielectric properties: the intrinsic contribution, which is related to the ferroelectric (antiferroelectric) atomic structure, and the extrinsic contribution, which is associated with domains and defects.[1,2] In technologically important materials, such as $Pb(Zr,Ti)O_3$, the extrinsic factors can contribute as much as 70% to the total elasto-dielectric response (see Figure 1). Therefore, it is necessary to develop a greater understanding of all the possible defect and polarization mechanisms which could contribute to the extrinsic elasto-dielectric properties. However, a comprehensive theoretical description of the extrinsic contributions is currently not in place.

The most common mesoscopic structures associated with ferroelectric and related materials are domains and domain walls. Domains form at the phase transition and relate the low temperature phase to the high temperature prototype phase via certain symmetry constraints. In the example of "normal" first- or second-order ferroelectric transitions, each domain is an area of uniform polarization, and the boundary which divides two domains (i.e. a twin structure) is known as the *domain* wall. The domain wall is a region of distorted crystal structure in which there exists a spatial transition of the polarization from one orientation state to another.

There are two main types of twin structures. One type is a twin with inversion symmetry of the polarization but in which the strain is the same in both variants. The second type is a twin of two variants with different orientation for both polarization and strain. Ferroelectric twins are typically of the head to tail configuration. There are reports of other domain configurations, such as head-to-head types, but these have not been extensively investigated.[3,4]

The fine structure of the ferroelectric domain walls depends on a number of inter-related parameters: including the symmetry, temperature, order of the phase transition, spontaneous polarization, and the electrostrictive and elastic compliances. A number of analytical descriptions now exist to describe the spatial variation of the order parameter in a ferroelectric domain wall.[5,6,7] However, some of the parameters required by the theory cannot be easily acquired with current experimental techniques, and so there is a need to develop new experimental methods to study polarization variations in these materials.

Defects and dopants are known to have a strong influence on the elasto-dielectric properties of ferroelectrics and related materials. Theoretical treatments of the role of defects near structural phase transitions are usually restricted to defect densities that are much less than the reciprocal correlation volume ($\sim 10^{18}$ cm^{-3}).[8] In the perovskite ferroelectrics of commercial interest, such a situation is almost never realized.

This article outlines some of the results observed by diffraction contrast electron microscopy in perovskite-based ferroelectrics.[10] From these results, and requirements of the theoretical developments, there is an urgent need to experimentally investigate the polarization gradients, both within the domain region and in the region of the domain wall. Electron holography is discussed as a technique potentially capable of quantifying the polarization gradients in these materials.

Results and Discussion

La-doping in PZT-based Perovskites

Doping in $Pb(Zr,Ti)O_3$-based materials by lanthanum is used as a means to soften the switching characteristics of piezoelectric materials.[11] Additionally, the incorporation of lanthanum facilitates the fabrication of transparent ceramics for optoelectronic applications.[12] In general, doping with lanthanum has a significant influence on many of the elasto-dielectric properties. For sufficiently high levels of doping in Zr-rich PZT compositions, this leads to the observation of diffuse phase transition behavior having strong dielectric dispersion. Ferroelectrics with this behavior are generally referred to as relaxors, and are of technological importance owing to their unique electrostrictive, capacitive, and optoelectronic properties. The domain structures of relaxor $(Pb,La)(Zr,Ti)O_3$ (PLZT) ceramics are difficult to study using transmission electron microscopy. However, by carefully cooling a 8.2/70/30 composition, a microdomain contrast could be detected, as shown in Figure 2(a). Under the irradiation of the electron beam, the domain structure is unstable. By agitating the structure through focusing/defocusing the beam, the domain configuration transforms to a more stable ordered structure, Figure 2(b). It is believed that thermally-induced stresses switch the microdomain structure to a new domain configuration.[13]

The end-member of the PZT solid solution, $PbTiO_3$, has the highest transition temperature (T_c = 490 °C) and the largest strain [$(c/a - 1) \sim 6.5$ %] within the perovskite family. This makes $PbTiO_3$ an ideal material to study by transmission electron microscopy. Doping $PbTiO_3$ with lanthanum (PLT) reduces both the phase transition temperature and the characteristic discontinuity of the first-order transition. A systematic study of the structural effect of lanthanum on the polar domain structure in PLT ceramics reveals the development of a strain texture within the normal domains, Figure 3(a),(b),(c). Using diffraction contrast invisibility conditions, we were able to deduce that the texture is the result of a non-uniform spontaneous deformation along the *c*-axis within the domain. As shown in Figure 3(a), for a sample doped with 1 atom % La, there is no evidence of a texture. As the lanthanum concentration is increased from between 5 and 10 atom %, texturing appears, and this becomes progressively more pronounced with increasing dopant concentration. When the dopant concentration reaches 25 atom %, a normal domain structure is

not identified, and a full cross-hatched or "tweed" domain structure is observed below the transition temperature, Fig. 3d. Similar structures have been observed in ferroelastic systems such as $YBa_2(Cu_{0.9}Fe_{0.03})_3O_7$-δ and Mg- Cordierite.[14,15] Inhomogeneous polarization distributions are not unique to the PLZT system, but also exist in the complex lead $Pb(B'B'')O_3$ perovskite systems. In these systems, the intermediate scale B-site cation ordering is the source of the polarization modulation.[16] In order to further our understanding of the polarization variation in these materials, we need to develop a technique to quantify the polarization gradients and defect structures. In this regard, the potential of the electron holography technique is discussed below.

Electron Holography

The idea of using coherent electrons in electron microscopy was proposed in 1949 by Gabor in an attempt to extend the limits of electron microscope resolution.[17] However, the realization of electron holography was achieved only in the 1980's owing to the development of a coherent field-emission electron beam. Commercial instruments for electron holography have been developed by Hitachi Ltd. and Philips but have only recently become available. The principle of electron holography is similar to that of optical holography, in which the the phase and amplitude of the electron beam are recorded simultaneously. The addition of phase shift information which is highly sensitive to local changes makes electron holography a more attractive method compared to conventional electron microscopy techniques. There have been a variety of applications for this new technique starting since 1980, especially in the study of magnetic domains and fluxons in superconducting materials.[18]

Recently the possibility of using the holography technique to study ferroelectric domain walls and other defect structures in ferroelectrics was recognized. Some encouraging results have been reported on the profiles of domain walls, as shown in Figure 4.[19] The kink-like electron interference fringe pattern closely resembles the space profile of the polarization vector across a domain wall as predicted by the Landau-Ginzburg model.[5,6] Although a complete theoretical description of the fringe profile in Ref. 18 is not currently available, the fact that the electric field variation can be probed on a scale less than 1 Å is both exciting and promising.

It has been demonstrated that the electron holography technique may also be used to study the location of aliovalent dopants inside crystal structures through the perturbed local electric fields.[20] As shown in Fig. 5a the fringe bifurcations occurred across the domain wall. Potential contours reveals there are charge centers attracted to the domain wall (see Figure 5b).[20] This information may lead to a significant advance in the understanding of the effect of dopants, and may shed new light on the study of interactions between the dopants and domain walls and other polarization modulations as described above.

Quantitative study of the polarization profiles can have a significant impact on the fundamental understanding of ferroelectrics. Once the relationship between the fringe variation and the polarization space profile is established, one can obtain the polarization gradient coefficients through back fitting the observed domain profiles to the theoretical results on domain walls.[7] These gradient coefficients are a measure of the nonlocal coupling strength. Using lattice dynamics, one may correlate these gradient coefficients to the dispersion surface near the soft mode of the paraelectric-ferroelectric phase transition.[21] Hence, the electron holography technique, together with the continuum model described in Ref. 6, can potentially provide a methodology to study the characteristics of the over-damped soft mode in systems such as $BaTiO_3$, which could not be directly probed through inelastic neutron scattering.

As a new technique, many problems still exist in the electron holography, especially with regard to the interpretation of the observed fringes. In principle, the total phase shift of high energy coherent electrons passing through a ferroelectric thin sample may be calculated from the following equation[22]

$$\phi(x_0,y_0) = \frac{\pi}{\lambda\Sigma}\int V(x_0,y_0,z)dz, \qquad (1)$$

where λ is the electron wavelength, x_0 and y_0 define the point on the thin sample, Σ is the electron energy, and $V(x_0,y_0,z)$ represents the electrical potential experienced by the traveling electrons. However, $V(x_0,y_0,z)$ represents the total potential, and it is quite difficult to delineate contributions from the "bound" charges (relevant to the polarization) and the "free" charges (relevant to compensation). We believe this is the main reason for the inconsistencies encountered in the current studies of ferroelectrics using electron holography.[23] More theoretical analysis of the interpretation of the holography results is in order.

Conclusions

Observations by conventional transmission electron microscopy techniques on ferroelectric and related materials reveal a variety of polarization modulations which can be induced when there exists coupling of the primary order parameter to symmetry breaking defects. From the evolution of the modulated structures and domain structures, one can see some link between these mesoscopic structures and the extrinsic elasto-dielectric properties.

A new electron-microscopy technique using coherent electrons known as electron holography opens up opportunities in the study of domain walls and defect structures. In this technique, phase shifts can be correlated to local variations of the electrostatic fields within materials. Further development of this new technique in the study of ferroelectrics may help us to

gain new insight into the mechanisms of extrinsic contributions to the macroscopic elasto-dielectric properties.

Acknowledgements

We wish to thank the ONR via Grant No. N00014-89-J-1689 and the AFOSR via Gant No-91-0433 for partly funding this program. We also wish to thank Drs. D. C. Joy, Xiao Zhang, and Larry Allard for many useful conversations regarding electron holography and Dr. L.E. Cross for discussions on ferroelectrics in general.

References:

1 M. Marutake, J. Phys. Soc. Japan, **11**, 807 (1956).

2 A. G. Luchaninov, L. Z. Potikha and V. A. Rogozin, Zh. Tekh. Fiz., **50**, 616 (1980).

3 S. I. Yakunin, V.V. Shakmanov, G. V. Spivak and N. V. Vasileva, Sov. Phys. Solid State, **14**, 310 (1972).

4 C. A. Randall, D. J. Barber, and R. W. Whatmore, J. Mat. Sci., **22**, 925 (1987).

5 V.A. Zirnov, Sov. Phys. JETP **35**, 822 (1959).

6 W. Cao and L. E. Cross, Phys. Rev. B **44**, 5 (1990).

7 W. Cao and G. R. Barsch, Phys. Rev. B **41**, 4334 (1990).

8 A. P. Levanyuk and A. S. Sigov, in"Defects and Structural Phase Transitions" Gordon and Breach Science Publisher, New York (1987).

9 E. K. H. Salje, Acta Cryst., A **47**, 453 (1991).

10 P. Hirsch, A. Howie, R. B. Nicholson, D. W. Fashley, M. J. Whelan "Electron Microscopy of Thin Crystals" Robet Krieger Publishing Co. New York (1965).

11 B. Jaffe, W. R. Cook and H. Jaffe, in "Piezoelectric Ceramics" Academic Press Inc., New York (1971).

12 G. H. Haertling and C. E. Land, Am. Cer. Soc., **54**, 1 (1971).

13 C. A. Randall, D. J. Barber, and R. W. Whatmore, J. Microsc., **145**, 275 (1987).

14 Y. Zhu, J. Tafto and M. Suenaga, MRS Bul., **16**, 54 (1991).

15 E. K. H. Salje, Phase Transitions, **34**, 25 (1991).

16 C. A. Randall, A. S. Bhalla, T. R. Shrout and L. E. Cross, J. Mat. Res., **5**, 829 (1990).

17 D. Gabor, Proc. R. Soc. London, Ser. A. **197**, 454 (1949).

18 see the review article by A. Tonomura, Rev. of Mod. Phys., **59**, 639 (1987) and the references thereafter.

19 X. Zhang, T. Hashimoto, and D.C. Joy, Appl. Phys. Lett. **60**, 784 (1992).

20 X. Zhang and D. C. Joy, Presentation in Materials society Meeting, Boston, Massachusetts, 1992.

21 W. Cao, to be published.

22 G.F. Missiroli,G. Pozzi, and U. Valdré, J. Phys. E **14**, 549 (1981).

23 W. Cao and C. A. Randall, Solid State Comm., **86**, 435 (1993).

Figure Captions

Figure 1. Temperature dependance of the dielectric permittivity of doped-PZT ceramics. The theoretical value from the Landau-Devonshire theory is also shown.

Figure 2. (a) Bright field image of liquid nitrogen cooled PLZT 8.2/70/30 relaxor ferroelectric revealing a microdomain structure. (b) An *in situ* switched pseudo-domain structure of (a).

Figure 3 Bright field image of domain structures in a solid solution series $(Pb_{1-3x/2}La_x)TiO_3$ with four different La contents.

Figure 4 An electron hologram of a 90° domain wall in $BaTiO_3$, the fringe bending is related to the polarization difference across the domain wall (ref. 19).

Figure 5 (a) An electron hologram showing anomalous fringe bifurcations in a 90° domain wall in $BaTiO_3$. (b) Electron interferogram of the same area of (a) shows charge defect centers within the wall (courtesy of Drs. D. Joy and X. Zhang).[20]

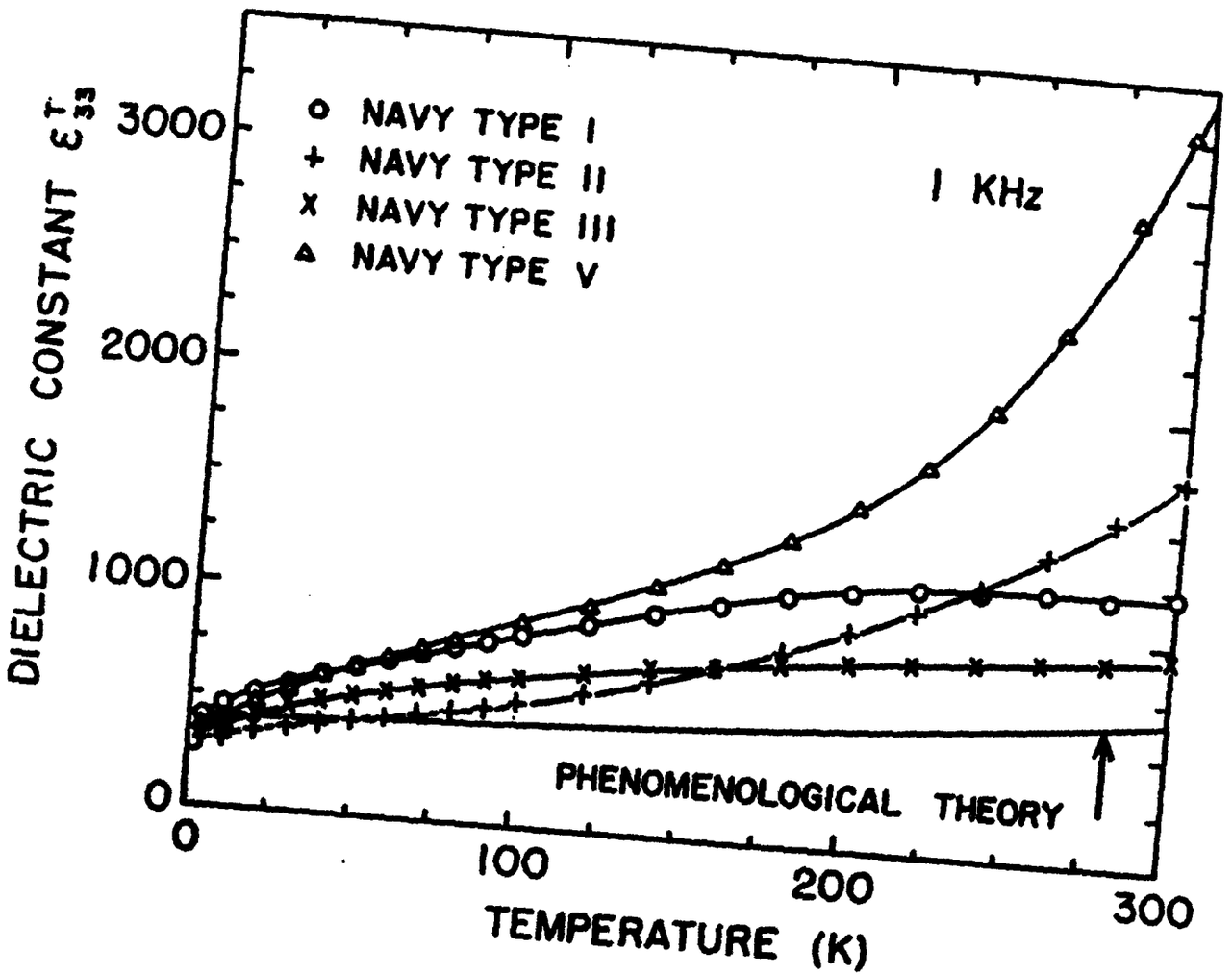

Fig. 1

Randall/Ferroelectrics

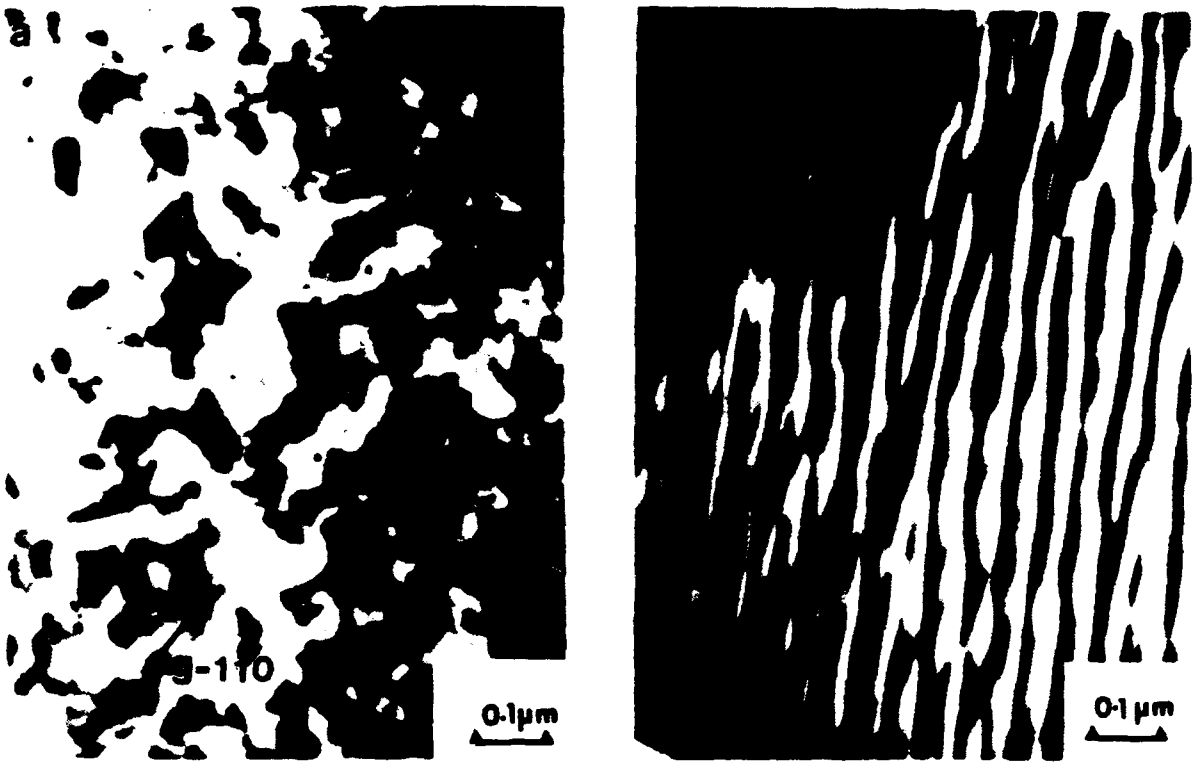

Figure 2

Randall/Ferroelectrics

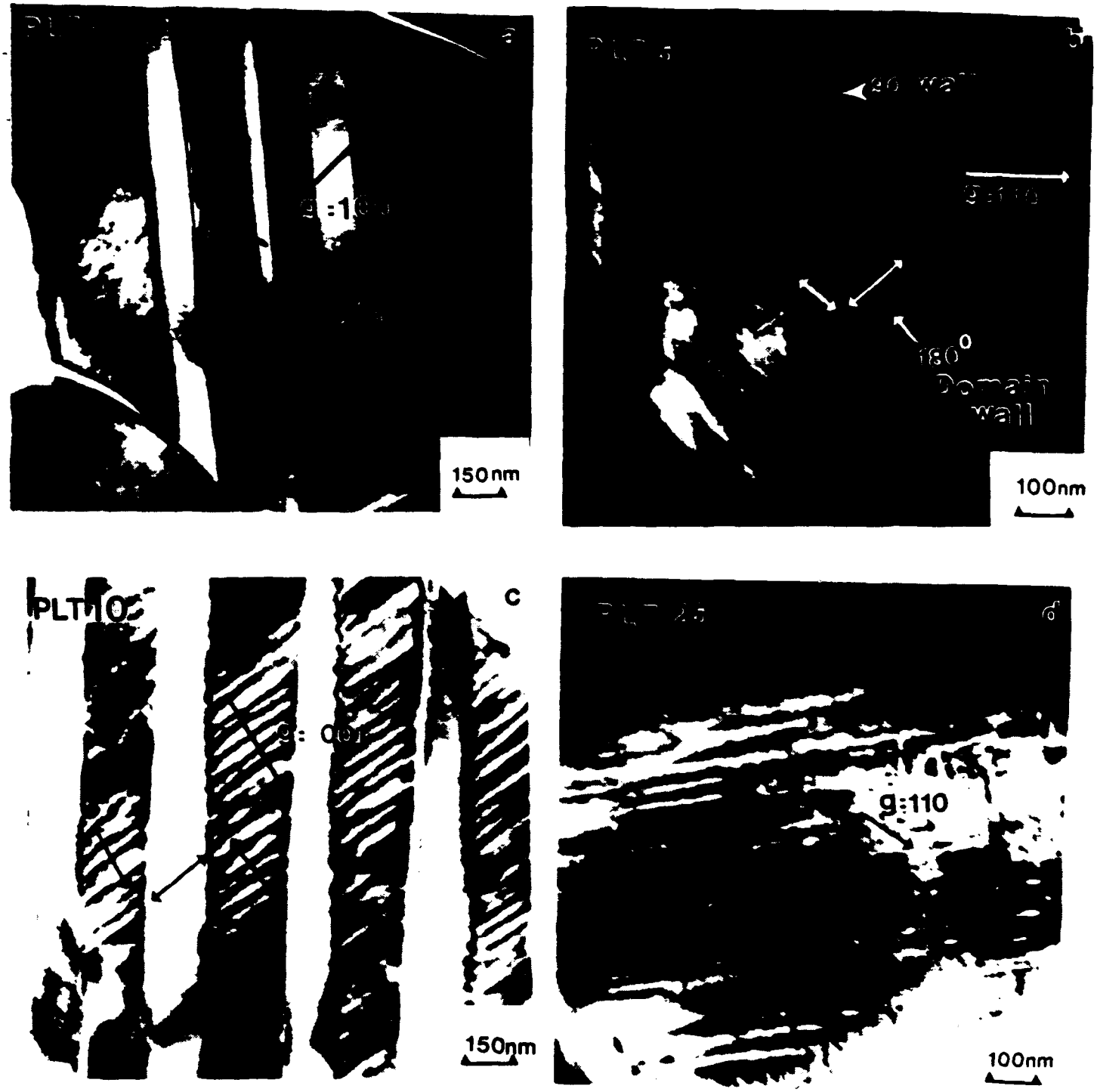

Figure 3

Randall / Ferroelectrics

Figure 4

Randall/Ferroelectrics

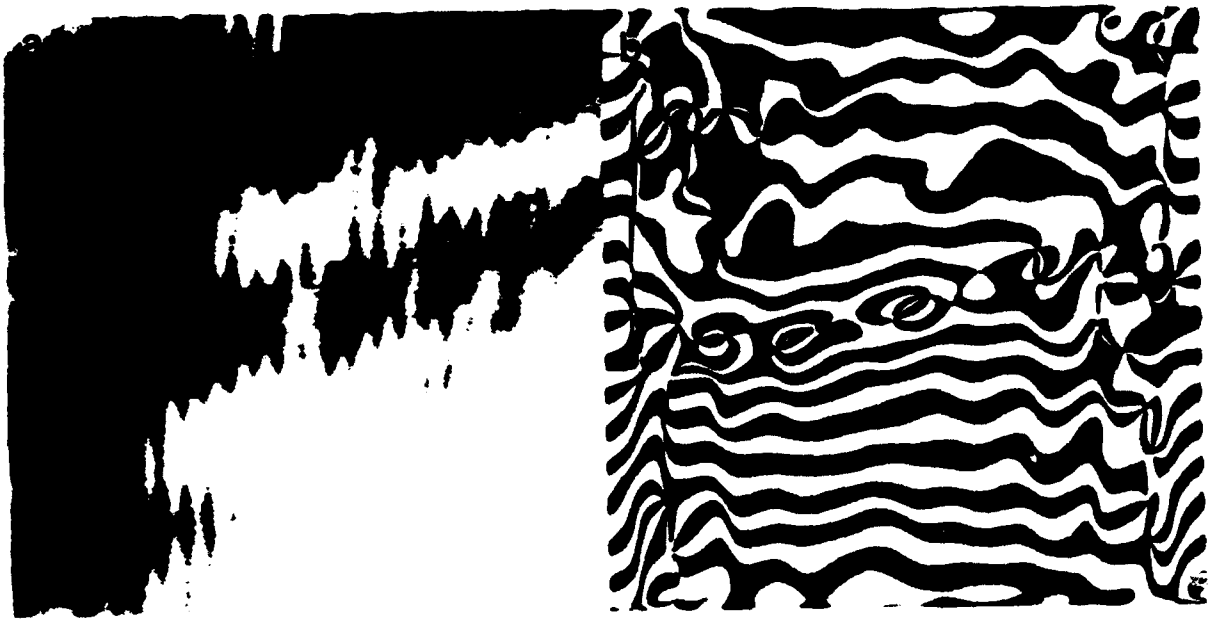

Figure 5

A4

MICROSTRUCTURAL CHARACTERISTICS AND DIFFUSE PHASE TRANSITION BEHAVIOR OF LANTHANUM-MODIFIED LEAD TITANATE

G. A. ROSSETTI, JR†., W. CAO, AND C. A. RANDALL
Materials Research Laboratory, The Pennsylvania State University
University Park, Pennsylvania 16802
† Now with the Department of Geological and Geophysical Sciences and
Princeton Materials Institute, Princeton University, Princeton, New Jersey 08544

Abstract The introduction of structural disorder into perovskite ferroelectrics leads to the observation of diffuse phase transition behavior. In this paper, the microstructural characteristics and phase transition behavior of lanthanum-modified lead titanate are discussed. It is shown that the diffuse nature of the transition is connected with the appearance of ferroelectric domain structures exhibiting texture on the mesoscopic (≈ 10 nm) length scale. The theoretical implications of these results are briefly discussed.

INTRODUCTION

Diffuse phase transitions in perovskite ferroelectrics occur as a consequence of some level of structural disorder that breaks the translational invariance of the lattice. The type of diffuse transition observed depends both on the nature and scale of the structural disorder. Impurities, point defects, extended defects, incomplete or inhomogeneous cation ordering, macroscopic fluctuations in chemical composition, core/shell structures *etc.* can all lead to smearing of the ferroelectric phase transition. The physical origin of the smearing and the behavior of the ferroelectric properties in each particular case, however, may be very different. In chemically complex compounds and solid solutions, several types of structural disorder are often present simultaneously. To establish structure-property relations in these materials therefore requires characterization at all the relevant length scales, including the macroscopic (crystal symmetry, chemical homogeneity, core/shell structures), the microscopic (ferroelectric domain structures, extended defects), the mesoscopic (cation order domains, texture within ferroelectric domains), and the atomic (point defect chemistry, local environment).

For ferroelectrics such as lanthanum-modified lead zirconate-titanate (PLZT), the structural disorder arises as a consequence of the complex defect chemistry associated with the aliovalent A-site substitution of lanthanum[1]. Keizer, Lansink and Burggraaf[2] have shown that the nature of the ferroelectric transition in ceramic specimens of the end member $Pb_{1-\alpha y}La_yTiO_3$ (PLT) changes smoothly from that expected in a sharp first-order phase change to that of a diffuse transition as

the lanthanum concentration is increased. Figure 1 shows that, when characterized by the exponent γ in the generalized Curie-Weiss law, the anomalous dielectric behavior onsets at $y \approx 0.05$ and becomes typical of diffuse transitions (*i. e.* $\gamma \approx 2$) when $y > 0.23$. Although the numerical values of γ depend somewhat on the lead elimination factor (α) as well as on the grain size, the general trend towards increasingly diffuse behavior with lanthanum substitution is intrinsic.

In order to better understand how structural disorder evolves and relates to the dielectric properties in PLT, we have recently undertaken transmission electron microscopy (TEM) and powder x-ray/neutron studies, the details of which are reported elsewhere[3-5]. In this paper, we draw on these results and speculate on some possible interconnections between the microstructure, dielectric properties, and the phase transition behavior.

RESULTS AND DISCUSSION

High resolution X-ray diffraction studies[4] of sol-gel derived powders have shown that the addition of lanthanum to lead titanate results in broadened diffraction profiles showing a marked profile asymmetry. The degree of asymmetry can be quantified by fitting the profiles to split Pearson distributions[6]. The split Pearson function gives two values for the full width at half maximum, β^L and β^H, which are characteristic of the peak shape on the low and high angle sides of the peak maximum, respectively. Figure 2 shows that both the peak asymmetry and the peak breadth renormalize as a function of lanthanum concentration. The asymmetry (β^H/β^L) changes markedly between $y = 0$ and $y = 0.01$, but then decreases and becomes constant for samples with $y > 0.05$. At the same time, the profile breadth decreases. Corresponding to the changes in the diffraction profiles, the crystal tetragonality (*c/a*) begins to deviate from the linear composition dependence as expected based on Vegard's law. These observations cannot be easily explained by macroscopic variations in chemical composition, nor by particle size effects.

Alternatively, recent TEM studies[3] (Figure 3) reveal that the development of sub-domain texture in PLT materials closely parallels the changes observed both in the X-ray studies and in the dielectric behavior. For samples with $y < 0.05$, no sub-domain texture is observed, and the transition behavior is sharp. For samples with $y \geq 0.05$, sub-domain texture becomes apparent, and increases in degree with lanthanum concentration. As the sub-domain texture becomes more pronounced, the dielectric behavior near the transition becomes correspondingly more

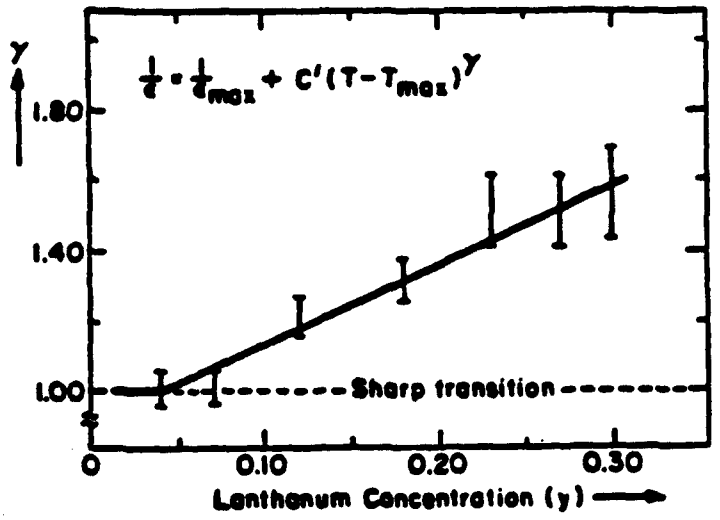

Figure 1. Composition dependence of the exponent γ in the generalized Curie-Weiss law for $Pb_{1-a}yLa_yTiO_3$ (After Reference 2).

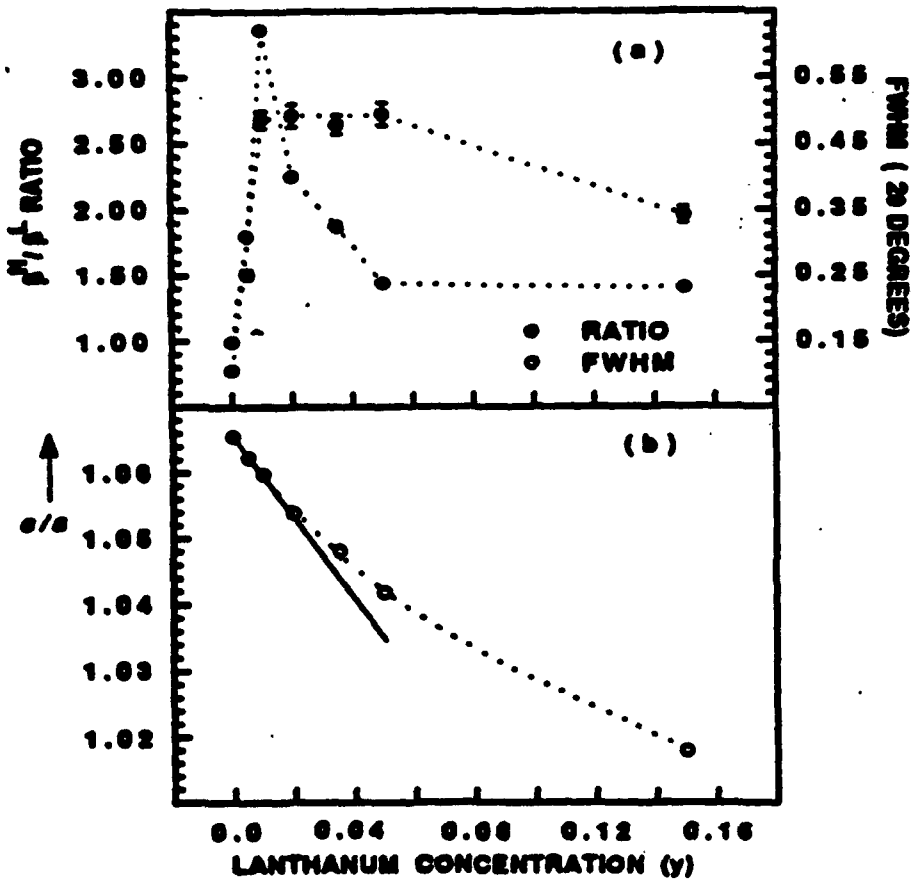

Figure 2. Breadth and asymmetry of the 002 powder XRD profile (a) and crystal tetragonality (b) of $Pb_{1-a}yLa_yTiO_3$.

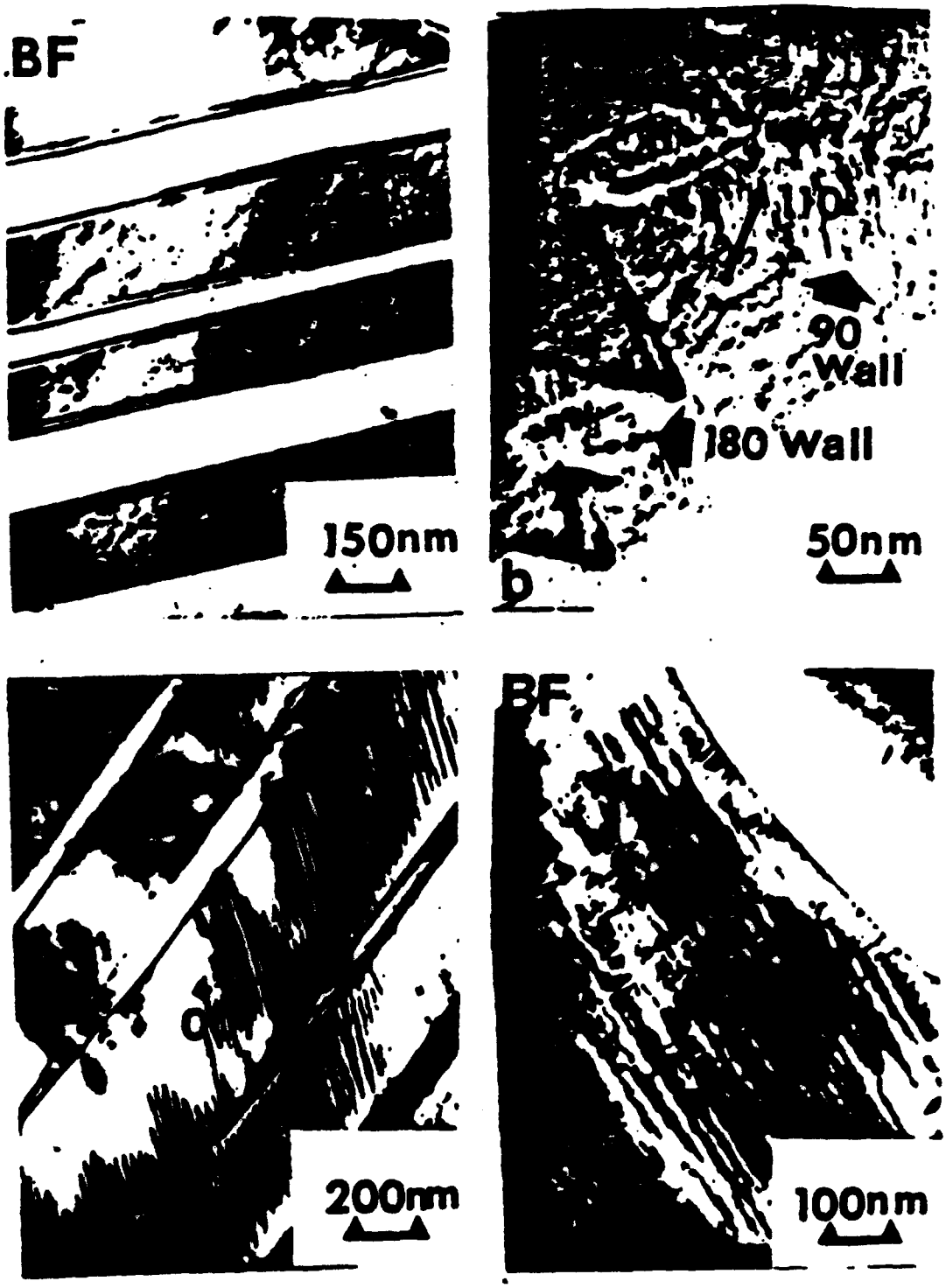

Figure 3. Transmission electron micrographs of $Pb_{1-ay}La_yTiO_3$: (a) y = 0.01 (b) y = 0.05 (c) y = 0.10 and (d) y = 0.25.

anomalous. For compositions with y > 0.25, the microstructure degenerates into a cross-hatched or tweed texture. For these compositions, the dielectric behavior is typical of that for diffuse phase transitions. Note that these textures disappear on heating above the transition temperature, and so cannot be identified with exsolution lamellae.

The tweed structures observed for the higher lanthanum concentrations would appear to be precursors for the mottled and poorly defined vestiges of sub-domain texture as observed for PLZT[7]. The Zr-rich PLZT compositions exhibit strongly frequency-dispersive diffuse transitions similar to those of the complex B-site perovskites such as $PbMg_{1/3}Nb_{2/3}O_3$ (PMN) and related compounds. In the later case, however, it is the cation order domains persisting on a ~10 nm length scale that lead to the breakdown of the ferroelectric domain structure[8-10]. The similarity in mesoscopic domain texture of the PLZT and PMN type materials[11-13] is intriguing, since at the atomic level, the origin of the structural disorder in these two materials is very different.

With regard to the nature of the phase transition in PLT, the first-order character also follows the changes in structural properties as revealed in the X-ray data. The development of a Landau-Devonshire[14] formulation for the phase transition in PLT requires the expansion coefficients to depend on spatial variables, which results in a distribution of transition temperature. As a macroscopic average, one expects that the first-order discontinuity of the transition will be drastically reduced as the transition becomes diffused. The Landau theory is valid, however, only when the sub-domain modulations are weak, otherwise the gradient related (Ginsburg) terms must be included. Using the methodology described previously[15], the coefficients in the Landau-Devonshire expansion were estimated for compositions with y < 0.05, where judging from Figure 3, this condition is approximately satisfied. As shown in Figure 4, the coefficient of the quartic term in the elastic Gibbs function (α_{11}^X) increases rapidly toward zero between y = 0 and y = 0.01 but then changes at a much lower rate. This increase reflects the apparent loss in the first-order character of the transition as the structure relaxes to the defects and the long range order is disrupted. The coefficient of the sixth-rank term also renormalizes, but to a much lesser extent. Large changes in the coefficient of the quartic term were also observed for PLZT compositions[16].

For the compositions with y > 0.05, the Ginsburg terms must be included in the formalism. The inclusion of the gradient energy can describe both the domains and their modulations. Periodic domain structures can be excited for a finite

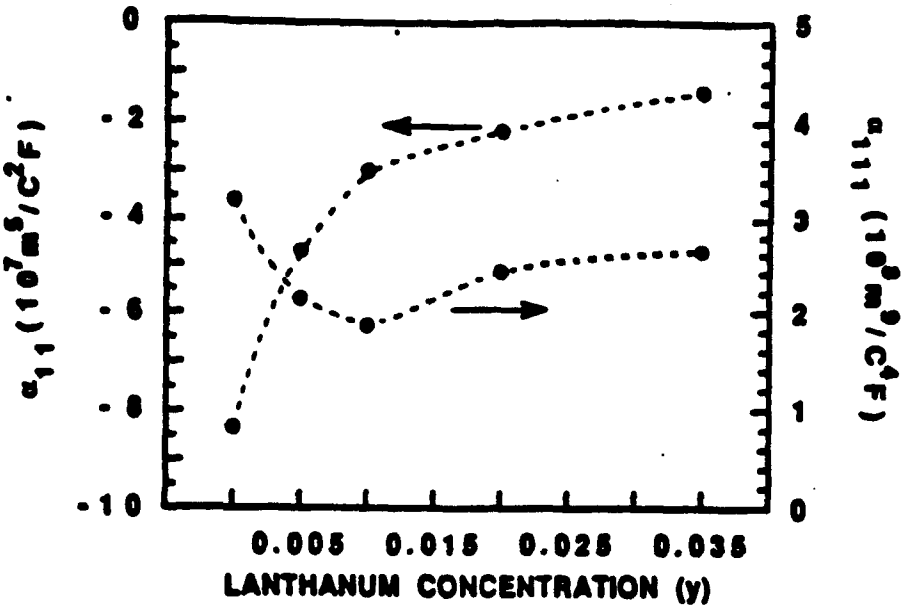

Figure 4. Coefficients of the elastic Gibbs free energy density function of $Pb_{1-\alpha y}La_yTiO_3$.

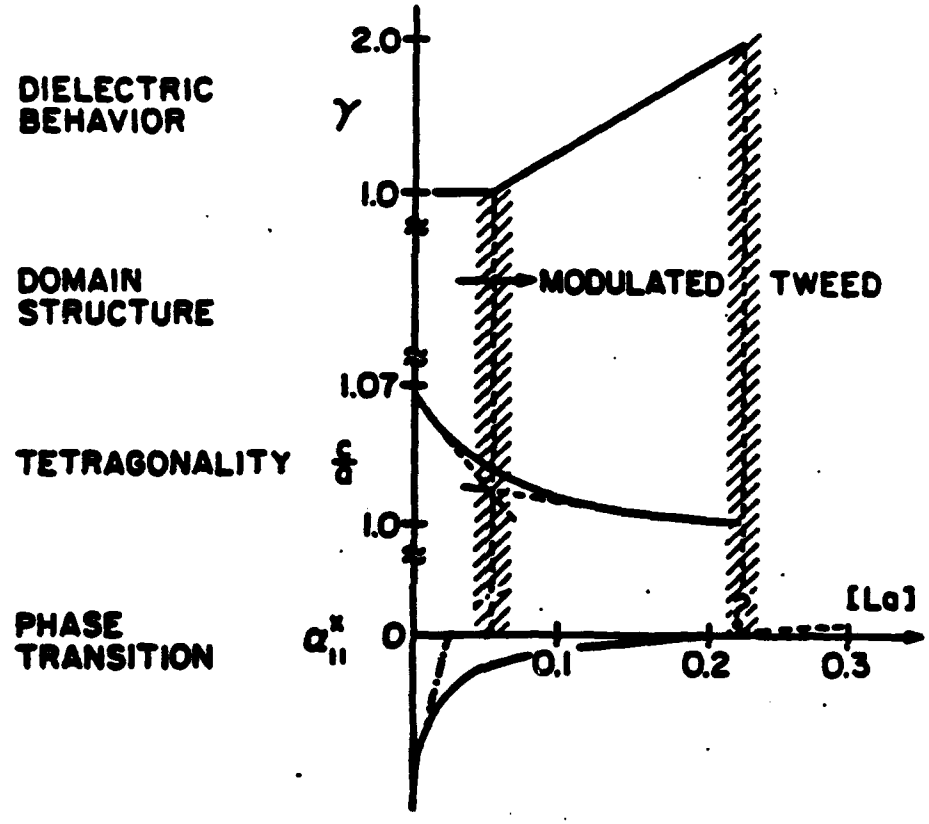

Figure 5. Observed relationships between the first-order character of the transition, the crystal tetragonality, the sub-domain texture, and the dielectric properties of $Pb_{1-\alpha y}La_yTiO_3$.

system due to the competition between nonlinearity and nonlocality. Modulated structures and tweed textures can be described in terms of crest riding periodons[17,18]. However, the modulated structures such as those in Figure 3c do not seem to follow the expected temperature variation pattern of the crest riding periodon excitations, which are unstable and can survive only in a finite temperature range near the transition. One possible explanation could involve an interaction of the defects with the periodons. These excitations might be stabilized by the lanthanum/vacancies if the defects are appropriately aligned. The alignment can be driven, on the other hand, by the field gradient created at the walls of the periodons. Consistent with this notion, the modulations have preferred orientations (although not perfect), and are nearly periodic, as shown in Figure 3. Further studies will be required to confirm this picture.

At the higher lanthanum concentrations ($y > 0.25$) the microstructure breaks down on still finer scales and more degenerate states are created. This will effectively increase the dielectric response of the system, as observed. For these materials, however, arguments based on the continuum theory as summarized above may not be used because the density representation (both in terms of energy and polarization) is no longer valid. Instead, discrete models must be developed. The results described above can be represented schematically as shown in Figure 5, where the observed relationships between the first-order character of the transition, the crystal tetragonality, the sub-domain texture, and the dielectric properties are shown. Here it is worth mentioning that, in the Landau-Devonshire formalism, close inter-relationships exist between the curvature of the energy surface, the order of the transition, and the symmetry of the ferroelectric phase. In this connection, it is of interest to consider how the scenario depicted in Figure 5 may change as zirconium, which lowers the tetragonality of the system and further flattens the energy surface, is added to the system. Based on the above discussion, we might expect that lanthanum will become more effective at breaking down the domain structure as the rhombohedral side of the PLZT diagram is approached, leading to a large number of degenerate states and additional contributions to the dielectric response even at modest lanthanum concentrations.

SUMMARY

The breakdown of conventional ferroelectric phase transition behavior in lanthanum-modified lead titanate has been correlated with the appearance of

domain structures exhibiting texture on a nanometer scale. It was suggested that this type of mesoscopic sub-domain texture is a common feature of ferroelectrics showing diffuse/frequency dispersive transitions. The theoretical implications of the relationships existing between the curvature of the energy surface, the order of the transition, the symmetry of the ferroelectric phase, the development of the sub-domain texture, and the resulting dielectric properties were discussed.

ACKNOWLEDGEMENT

This work was supported by contracts administered through the Office of Naval Research and a grant from the Air Force Office of Scientific Research. The authors are grateful to Professor L. E. Cross for his support of, and interest in, this study. Thanks also to Mr. N. Kim for fabricating the ceramic specimens used in the TEM studies.

REFERENCES

1. K. H. Härdtl and D. Hennings, J. Am. Ceram. Soc., 55 230 (1972).
2. K. Keizer, G. J. Lansink, and A. J. Burggraaf, J. Phys. Chem Solids, 39 59 (1978).
3. C. A. Randall, G. A. Rossetti, Jr., and W. Cao, Ferroelectrics (in press).
4. G. A. Rossetti, Jr., L. E. Cross, and J. P. Cline, J. Mater. Sci., (to be published).
5. G. A. Rossetti, Jr., M. A. Rodriguez, A. Navrotsky, L. E. Cross, and R. E. Newnham, Powder Diffraction, (to be published).
6. M. M. Hall, Jr., V. G. Veerarghavan, H. Rubin, and P. G. Winchell, J. Appl. Cryst., 10 66 (1977).
7. C. A. Randall, D. J. Barber, and R. W. Whatmore, J. Microscopy, 145 275 (1987).
8. H. B. Krause, J. M. Cosley, and J. Wheatly, Acta Cryst., C35 1015 (1979).
9. C. A. Randall, D. J. Barber, and R. W. Whatmore, J. Mater. Sci., 22 935 (1987).
10. C. A. Randall and A. S. Bhalla, Jap. J. Appl. Phys., 29 327 (1990).
11. C. A. Randall, D. J. Barber, R. W. Whatmore, and P. Groves Ferroelectrics, 76 265 (1987).
12. A. D. Hilton, C. A. Randall, D. J. Barber, and R. W. Whatmore, Inst. Phys. Conference Series, No. 90, Chapter 9, 315 (1987).
13. A. D. Hilton, C. A. Randall, D. J. Barber, and T. R. Shrout, Ferroelectrics, 93 379 (1989).
14. A. F. Devonshire, Advances in Physics, 3 85 (1954).
15. G. A. Rossetti, Jr., Ferroelectrics, 133 103 (1992).
16. G. A. Rossetti, Jr., T. Nishimura, and L. E. Cross, J. Appl. Phys., 70 1630 (1991).
17. G. R. Barsch and J. A. Krumhansl, Met. Trans. A., 19A 761 (1988).
18. W. Cao , J. Phys. Soc. Japan, in press (1994).

DOMAIN PROCESSES IN FERROELECTRIC CERAMICS

TECHNICAL REPORT FOR THE FIRST YEAR

Period October 1, 1991 to September 30, 1992

by

L. E. Cross and Wenwu Cao

AIR FORCE OFFICE OF SCIENTIFIC RESEARCH

Grant No AFOSR-91-0433

PENNSTATE

THE MATERIALS RESEARCH LABORATORY
UNIVERSITY PARK, PA

TABLE OF CONTENTS

I. INTRODUCTION

This is the progress report for the first year of a two year program sponsored by the Air Force Office of Scientific Research on "Domain Processes in Ferroelectric Ceramic". Domain processes contribute a large portion in the dielectric and piezoelectric activities in ferroelectric ceramics, a better understanding of this subject can be of great help in future materials development tor acoustic devices and smart structures. The materiai studied in the first year investigation is the $PbZrO_3$-$PbTiO_3$ solid solution, the so called PZT ferroelectric ceramic, which has been the primary transduce material for the past thirty years. Although PZT is a well known transducer material and has been used widely, there has not been any systematic theoretical study in the past, which unambiguously characterizes this system, especially lacking the knowledge on the mechanism for the strong piezoelectric activities. Only in the last few years people have started to realize that the major contributor in the piezoelectric effect is from the domain processes and have made a start to distinguish and separate the intrinsic and extrinsic contributions. Our focus in this project is to understand, from a theoretical point of view, the extrinsic contributions. In the first year of this Air Force sponsored program, we have carried out a critical study on the PZT system and found many ill-defined concepts and definitions. Among these are the concept of the morphotropic phase boundary (MPB), the distribution of coexisting phases in a complete solid solution system, the distinction between domain switching and field induce phase transition, and the relationship between antiphase boundaries and ferroelectric domain walls in the rhombohedral II phase. These problems have been addressed in the first year and the details are given in the following sections II, III and IV, respectively. A recently funded University Initiative Research (URI) program by the Office of Naval Research provided a solid back up on the experimental part of this study. Collaborative work between the two programs is already in progress (see section IV).

II. STUDY ON THE MORPHOTROPIC PHASE BOUNDARY IN PZT

The most useful PZT compositions are those near the so called Morphotropic Phase Boundary (MPB). The MPB is defined as a compositional phase boundary at which the free energies for the rhombohedral and tetragonal phases are equal. It is well known that many physical properties peak at the MPB, [1] but the reason for this is not well understood. In addition, the free energy is not a directly measurable quantity, in order to study the MPB we need to correlate the equal free energy concept to some measurable quantities. In the past, thermodynamic concepts developed for liquid-solid transition and liquid (or gas) mixtures were borrowed to address the MPB and the distribution of structural phase mixture in the PZT system. As a result, some inconsistencies and confusions are created. In light of this situation, we have conducted a systematic theoretical study on the MPB in the PZT system during the first year of this project.

A. The Definition of MPB

As pointed out in Appendix I that the MPB is conventionally represented by a nearly vertical line on the phase diagram (see figure 1 in Appendix I). In the classical book on piezoelectric ceramic by Jaffe Cook and Jaffe,[1] the MPB line is measured by X-Ray diffraction technique. The nearly vertical line on the phase diagram in the vicinity of 52/48 Zr/Ti ratio is obtained according to the criterion of equal volume fraction of the tetragonal and rhombohedral phases. In a liquid (or gas) mixture, the equal volume criterion can be derived from thermodynamic principles for an equilibrium system. However, for the structural phase mixture (which may not even be in thermodynamic equilibrium), the two phases derived from a common parent phase have different degree of freedom in the configurational space. It is shown in Appendix I that the MPB defined according to equal free energy criterion should not have equal volume fraction for the two coexisting phases if the geometrical constraints are imposed. Because the two low temperature phases are derived from the same cubic phase, in order to calculate the volume fractions we must study the actual transition process and include the structural constraints in the transition probability

calculation. It is shown (see Appendix I) that the volume ratio for the rhombohedral/tetragonal phases should be 60:40 at the MPB instead 50:50 used before.

B. Phase Mixing in Complete Solid Solution System

As shown in the phase diagram (see figure 1 of Appendix I) PZT is a complete solid solution system in the cubic phase. There is a paraelectric-ferroelectric phase transition which occur at around 370 ° C for the MPB composition. In such low temperature regime, there is no chemical driving force for phase separation to occur in this system. At the transition, the system only experiences a displacive structural distortion which produces a spontaneous polarization due to the relative shift of the positive and the negative charge centers. X-ray diffraction shows that the symmetry of the low temperature ferroelectric phase could be either tetragonal or rhombohedral, depending on the Zi : Ti ratio in the system. Near the MPB composition, the low temperature phase is a mixture of the tetragonal and rhombohedral phases. In an attempt, the fraction of each low temperature phase was described by the lever rule and the two edge compositions were fitted from the experimental data.[2,3] Although the fitting appears to be quite good, the edge compositions, which specify the width of the coexistence region, can not be uniquely determined, width of the coexisting region ranging from 0 to 20 mole percent. It is found that in general ceramics of smaller grain size have larger coexistence region and ceramics of larger grain size have smaller coexistence region.

We have looked into this problem in more detail and found that the description of the phase coexistence in PZT using the lever rule is actually in contradiction with the nature of the complete solid solution system, because the two edge compositions in the lever rule actually specify a solubility gap. Since such solubility gap does not exist in the PZT system, naturally one can not define these two edge compositions using the lever rule. Considering the fact that the paraelectric-ferroelectric phase transition is second order for PZT at compositions near the MPB, we propose that the phase coexistence in this system is a result of a "frozen in" metastable phase from thermal

fluctuations at the paraelectric-ferroelectric phase transition (see Appendix II). A method is introduced to calculate the fractions of the two "frozen in" phases, which takes into account both the structural constraints and the statistics. The theoretical calculations agree well with the experimental results. More importantly, the new model does not contain the two fixed edge compositions as in the lever rule, instead, two new variables are introduced: one is the MPB composition which is a fixed quantity, and another is the width of the coexistence region which is inversely proportional to the volume of the particles (or grains). The new model not only is compatible with the nature of solid solution system but also can explain the grain size dependence of the coexistence region observed experimentally. Although the quantitative test of the new model awaits more refined experimental input, we believe that the conceptual breakthrough is significant and could trigger further development on this subject.

III STUDY THE PHASE TRANSITION IN RHOMBOHEDRAL PHASE PZT AND ANTIPHASE STRUCTURE IN R3c PHASE

As part of the first year effort we have initiated a joined investigation on the PZT system with the Navy supported URI program . The focus is on the R3m → R3c phase transition in the rhombohedral ferroelectric phase of PZT. This phase transition is not well understood in terms of the Landau-Devonshire formalism. In addition to the soft zone center mode, there exists another soft zone boundary mode which involves the tilting of the oxygen octahedra in the perovskite structure and causes unit cell doubling. We have made a detailed structural study using Transmission Electron Microscopy. One of the most interesting findings is that many antiphase boundaries are generated in the R3c phase and these antiphase boundaries are, in most cases, not confined by the crystal symmetry (see Appendix III). The antiphase boundaries with their orientation compatible with the crystal symmetry have been addressed by Cao and Barsch,[5] but the observed antiphase boundaries in the PZT system seem to be not confined by symmetry at all. We suspect that there are two different kinds of antiphase boundaries in the R3c phase of PTZ, in

one kind the boundaries are orientated along the polarization direction and the other kind with their orientation perpendicular to the polarization. The observed antiphase boundary may be the combination of the two. Modeling of the antiphase boundary along this line is currently in progress.

PZTs of the rhombohedral symmetry is one of the best pyroelectric materials. Unfortunately, the existence of this R3m → R3c phase transition produces a second kink in the polarization versus temperature plot, which effectively limits the temperature range in real applications. The understanding on this transition process and the associated domain structures could help to overcome this hindrance.

IV. PAPERS PRESENTED AT NATIONAL AND INTERNATIONAL MEETINGS

1. Wenwu Cao and L. E. Cross "Elastic Compatibility and Charge Neutrality in the Domain Structures of Ferroelectrics" American Physical Society March Meeting, Indianapolis, Indiana, 1992.

2. Wenwu Cao and L. E. Cross "Ratio of the Rhombohedral and Tetragonal Phases on the the Morphotropic Phase Boundary in Lead Zirconate Titanate", The Eighth International Symposium on the Applications of Ferroelectrics, Greenville, SC. August 31-Sep. 2, 1992.

3. L. E. Cross and Q. Jiang "Fatique Effects in High Strain Actuators" Second Joint US-Japan Conference on Adeptive Structures, Nagoya, Japan, Nov. 12-14, 1991.

4. L. E. Cross "Ceramic Sensors and Actuators for Smart Structures" Indo-US Workshop on Perspective in New Materials, March 23-24, 1992.

5. L. E. Cross"Ferroelectric Ceramic Sensors and Actuators for Smart Composites and Adeptive Structures ECAPD2, London, April 12-15, 1992.

V. HONORS TO FACULTY AND STUDENTS

L. E. Cross, Orton Lecture, April 13, 1992. American Ceramic Society Meeting.

L. E. Cross, Materials Research Society Medal and Award, 1992.

VI. PROGRAMS IN PROGRESS

Several important issues have attracted our attention through the first year investigation. However, due to the limitation of manpower, it is not possible to address all of them. Currently, based on the already achieved progress, we are pursuing the following topics:

a) Study the periodic structure of domains in ferroelectric systems. This includes theoretical study on the relationship between the periodicity and the width of domain walls, particularly in PZT system. The theoretical study will also address the grain size dependence of the domain period, which can shed some light on the different domain patterns obtained from Transmission Electron Microscopy.

b) Study the octahedra tilt transition in the rhombohedral phase of PZT and the symmetry relation of the antiphase boundaries in the R3c phase to interpret the TEM results reported in Appendix III.

c) Extend the model described in Appendix I and II to incorporate the effect of external electric field. The change of distribution under an electric field will facilitate the calculation on the extrinsic contributions from the field induced phase transitions.

d) Enhance the link between this program and the Navy funded URI program and try to integrate the theoretical results with the experimental results. It is expected that the experimental work of the URI program will catch up in the coming year.

REFERENCES

1. B. Jaffe, W. R. Cook and H. Jaffe, Piezoelectric Ceramics, Academic Press, London (1976).

2. Lu Hanh, K. Uchino and S. Nomura, Japanese J. Appl. Phys., 17, 637 (1978).

3. P. Ari-Gur and L. Benguigui, Solid State Comm., 15, 1077 (1974).

4. Wenwu Cao and G. R. Barsch, Phys. Rev. B, 41, 4334 (1990).

Jpn. J. Appl. Phys. Vol. 31 (1992) pp. -
Part 1, No. 5A, May 1992

The Ratio of Rhombohedral and Tetragonal Phases on the Morphotropic Phase Boundary in Lead Zirconate Titanate

Wenwu CAO and L. Eric CROSS

Materials Research Laboratory, The Pennsylvania State University, University Park, PA 16802, U.S.A.

(Received November 13, 1991; accepted for publication March 7, 1992)

A method is introduced to determine the statistical distribution of energetically degenerate but geometrically inequivalent states in a temperature induced phase transition in solids. The method has been employed to calculate the ratio of the rhombohedral and tetragonal phases in the $Pb(Zr_xTi_{1-x})O_3$ solid solution of the morphotropic phase boundary (MPB) composition. Our results indicate that the MPB determined by Jaffe, Cook and Jaffe [*Piezoelectric Ceramics* (Academic Press, London, 1971) p. 136] from structural measurements should be shifted to the rhombohedral side, which is more consistent with the MPB determined from dielectric measurements.

KEYWORDS: ferroelectric ceramic, PZT, lead zirconate titanate, morphotropic phase boundary

A phase diagram representing the subsolidus phase relations in the system $PbZrO_3$-$PbTiO_3$ taken from the book by Jaffe, Cook and Jaffe[1] is given in Fig. 1. The system contains the well known solid solution series $Pb(Zr_xTi_{1-x})O_3$ (PZT) which exhibits a variety of phase changes. In this system the most interesting compositions are for those on or near the so-called morphotropic phase boundary (MPB) (see the nearly vertical line on Fig. 1). PZTs in this compositional region have superior piezoelectric properties and are the primary materials currently used in most piezoelectric transducers and actuators. As shown in Fig. 1 the ferroelectric phase is rhombohedral on the left-hand side and tetragonal on the right-hand side of the MPB line, respectively (note: there should be a co-existence region of the two phases which is not shown in this phase diagram). The MPB in Fig. 1 as quoted from the book (Jaffe, Cook and Jaffe, p. 136) "is considered as that composition where the two phases are present in equal quantity".

The MPB drawn on a phase diagram is a compositional boundary which is defined as the composition for which the free energies of two adjacent phases are equal. From thermodynamics, the free energy of a solid solution system depends on the following variables: temperature, pressure and composition. The compositional variable in the PZT case has a special property, it can only be directly accessed in certain temperature range. Out of that temperature range, the compositional variable can not be changed while keeping other variables fixed, as we know that a PZT solid solution can not be formed at room temperature. In order to change the composition at room temperature, one has to first heat up the system so that a single phase solid solution can be formed, then cool the system back down to room temperature after the new composition is formed. This special property of the compositional variable prevents direct thermodynamic analysis with this variable, and hence invalidates the transition hysteresis argument[2] in the explanation of the coexistence of two phases. Although the phase transition from the rhombohedral structure to the tetragonal structure must be of first order, it can not be realized while keeping the temperature unchanged, because the composition is not a directly accessible thermodynamic variable below a certain temperature limit. This is to say that we should address the temperature induced transition process in order to understand the effects of changing composition below a certain temperature limit.

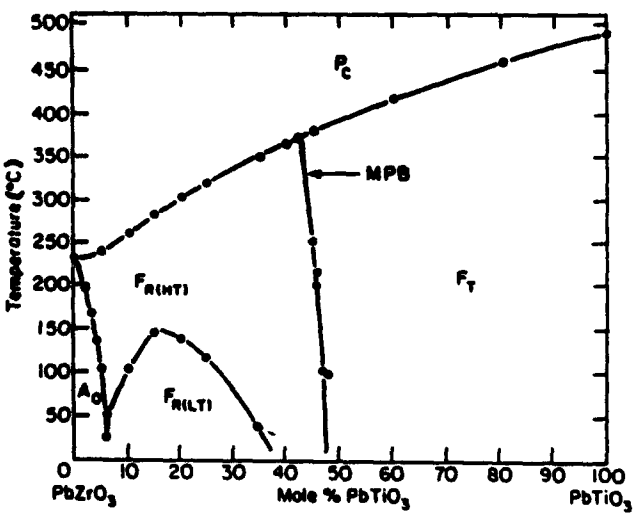

Fig. 1. Phase diagram of $Pb(Zr_xTi_{1-x})O_3$ [after Jaffe, Cook and Jaffe, ref. 1].

There are two types of phase mixing: one is the mixing of phases of different chemical compositions and the other is the mixing of phases with different structures but identical chemical compositon. At a first glance, it appears that the two problems seem to be similar, but they actually have quite different nature. The former reflects the law of mass conservation (obeying the lever rule), but the latter is actually a statistical distribution problem. It is the intention of this paper to provide a simple method dealing with the latter case.

From thermodynamic analyses, it is shown that the paraelectric-ferroelectric transition for compositions near the MPB is of second order within the experimental

error,[3] we therefore expect strong thermal fluctuations to occur near the transition temperature T_c. This thermal fluctuation is the sole driving force for the phase transition. For convenience we will work in the order parameter space. When the system is cooled down near T_c from the paraelectric phase, the magnitude of the thermal induced instant polarization $|P_{inst}|$ increases as the potential well around $P=0$ becomes flatter and flatter. Below T_c, the fluctuation is gradually frozen and the system acquires a new configurational state with a finite polarization. In a second order phase transition the transition process happens in a continuous fashion; but in a first order phase transition, a finite spontaneous polarization is obtained at the phase transition. The two cases are illustrated in Fig. 2 for a one-dimensional system, where the shaded area represents the level of thermal energy. In a one-dimensional system the number of allowed (two) orientations of the instant polarization is the same as that of the spontaneous polarization. But in two- and three-dimensional systems, there are no orientational constraints for thermal fluctuation (determined by the dimensionality of the problem only) although the magnitude of P_{inst} is regulated by the potential well around the origin. However, the allowed orientations for the spontaneous polarization P_s are limited. The thick line and the solid dots in Fig. 3 illustrated this situation for a two-dimensional problem representing a square to rectangular ferroelectric phase transition. There are no orientational constraints for P_{inst} in the fluctuating state [profile is represented by the thick line in Fig. 3(a)] but only four orientations for P_s [solid dots in Fig. 3(b)] are allowed well below T_c.

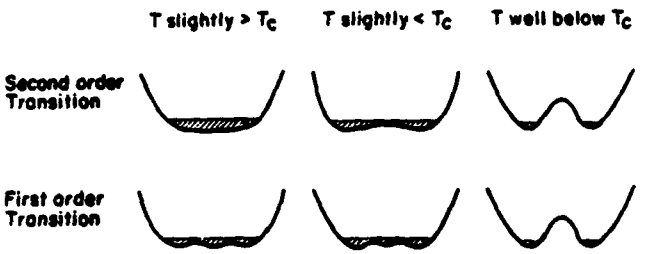

Fig. 2. Illustration of the potential wells and thermal fluctuations near the critical temperature T_c for both second and first order phase transitions in one dimension. The shaded areas represent thermal energy.

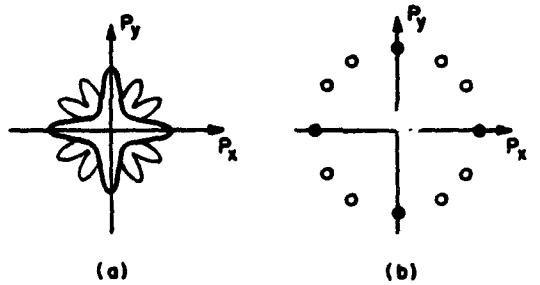

Fig. 3. Representation of fluctuating state and the ferroelectric states in order parameter space for a two-dimensional problem. (a) The thick and the thin lines are the profiles for the polarization fluctuations of the square-rectangular and square-oblique phase transitions, respectively, near T_c. (b) The solid dots are the degenerated rectangular ferroelectric states and the open circles are the degenerated oblique ferroelectric states, respectively, well below T_c.

The question we try to address in this paper is: what is the probability ρ_i for the system in Fig. 3(a) to become the ith low symmetry ferroelectric states in Fig. 3(b)? For the two-dimensional problem mentioned above, the answer $\rho_i=1/4$ may be obtained intuitively since the four low-temperature rectangle states are completely equivalent, i.e., these states are energetically degenerate and structurally identical. But in more general situations, intuition fails to provide an answer, for instance, the case shown in Fig. 3 where the energetically degenerated rectangle (solid dots) and the oblique (open circle) states are structurally different. In this case we need to follow a well-defined mathematical method to calculate these probabilities. Such a calculation is particularly useful for the study of PZT system, because at the MPB we have precisely such a situation, i.e., the tetragonal and rhombohedral phases are energetically degenerate.

It is obvious that the probability calculation is only meaningful in the fluctuating state. After the system being frozen into one of the low temperature states, thermal energy is no more effective to carry the system from one configuration to another. Our calculation is based on the following assumption:

The instant polarization P_{inst} is orientationally ergotic in the fluctuating state near T_c.

In other words, we assume that the thermal motion has no orientational preference, although as shown in Fig. 3, the magnitude $|P_{inst}|$ is regulated by the potential configuration and is a function of direction and temperature. An immediate inference from the assumption is that the average total polarization of the system is zero in the fluctuating state, or more concisely, $\langle P_{inst}\rangle=0$ but $\langle P_{inst}^2\rangle \neq 0$.

Now we try to correlate this thermal fluctuation with the transition probabilities to different structural phases. The assumption tells us that the trigger from the surrounding thermal bath is isotropic, but the actual structural change resulting from the trigger depends on the potential energy configuration. Because only a few isolated orientations for P_s are allowed below T_c in the order parameter space, we expect that all P_{inst} oriented in the vicinity of an allowed polarization direction can potentially develop into that final polarization state. Hence we can assign each allowed polarization state an effective solid angle Ω_i in a three-dimensional order parameter space, the probability ρ_i of that state being formed under the trigger of thermal fluctuation is represented by $\Omega_i/(4\pi)$, where 4π is the normalization constant.

The next task is to define the boundaries of these solid angles. Imagine we apply a small dc field E to lift the degeneracy of the system. Under this field the system will be forced to develop into one of the allowed low temperature states whose polarization vector has the smallest possible angle with the applied electric field. If this field is applied to the system from another angle, it can either in-

duce the same polarization state or a different state depending on whether or not the field is still oriented inside the effective solid angle of that state. Considering at a temperature slightly below T_c, there are two adjacent energetically degenerate states represented by P_a and P_b respectively, in the order parameter space (P_a and P_b form an angle Φ), the boundary of the two effective solid angles for these polarization states may be defined by

$$E \cdot P_a = E \cdot P_b \tag{1}$$

Taking the coordinate systems as shown in Fig. 4 we can write eq. (1) in the following form,

$$P_a \cos\phi = P_b \cos(\Phi - \phi). \tag{2}$$

Interestingly, the magnitude of the electric field has dropped out in eq. (2), hence if we take the limit $E \to 0$, the result in eq. (2) will still hold.

In reality, the problems of interest are those cases for which $P_a = P_b$, therefore, eq. (2) can be further simplified to

$$\phi = \Phi/2. \tag{3}$$

Equation (3) states that the boundary of two effective solid angles is a plane in the order parameter space passing through the bisector of the angle Φ and perpendicular to the plane containing P_a and P_b. If there exist more than two degenerate states, a boundary may be defined for each pair of adjacent effective solid angles using eqs. (2) or (3).

After the boundaries are defined, the remaining task becomes straightforward. We draw a polyhedron in the order parameter space surrounding the origin, whose edges are on the solid angle boundaries defined by eq. (3). For a PZT of MPB composition, the degenerated ferroelectric states include both rhombohedral and tetragonal phases. Assuming for the simplest case that $P_r = P_R = a$, then the corresponding polyhedron is shown in Fig. 5. The solid angle calculation can be written in terms of a surface integral on each of the corresponding surface which subtends that solid angle, for example

$$\Omega_{\square HIJK} = \iint_{\square HIJK} \frac{a\,ds}{(r^2+a^2)^{3/2}} = 4\int_0^b\int_0^b \frac{a\,dx\,dy}{(x^2+y^2+a^2)^{3/2}},$$
$$b = \frac{\sqrt{3}-1}{\sqrt{2}}a; \tag{5}$$

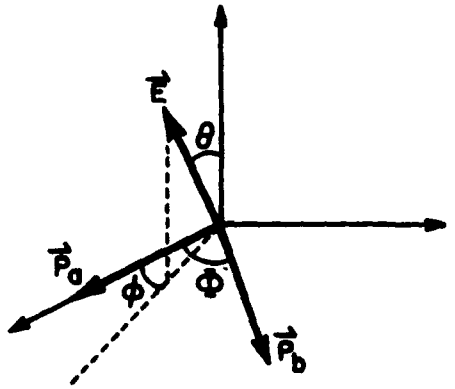

Fig. 4. Coordinate system used in the calculations of eqs. (2) and (3).

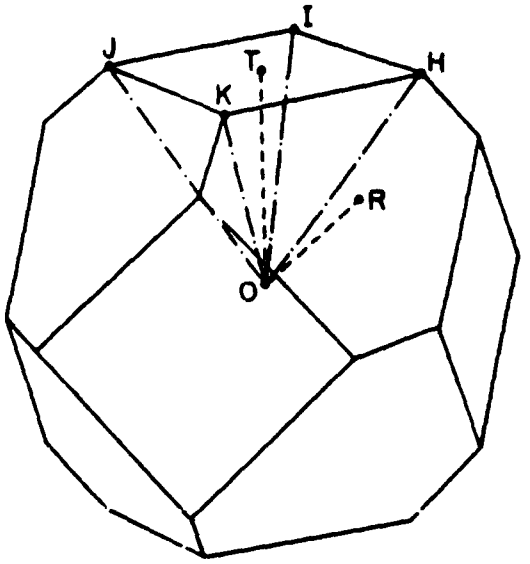

Fig. 5. The probability distribution polyhedron for PZT of the MPB composition, $\overline{OT} = \overline{OR}$. The solid angle subtended by the surface IIKH with respect to the origin O divided by 4π represents the probability of the system being transformed into $(00P_a)$ state.

where ds is the area element on the surface $\square$HIJK and r is the distance between ds and the center point T on that surface (Fig. 5). The integration of eq. (5) can be carried out to give an analytic solution

$$\Omega_{\square HIJK} = 4 \arcsin\left(\frac{3-\sqrt{3}}{6}\right). \tag{6}$$

From this result and the arguments given above we conclude that for PZT of the MPB composition, the probability ratio for a system to be frozen into rhombohedral and tetragonal phases from the fluctuating state is given by

$$\frac{\text{Rhombohedral}}{\text{Tetragonal}} = \frac{1-6\Omega_{\square HIJK}/4\pi}{6\Omega_{\square HIJK}/4\pi} = \frac{\pi - 6\arcsin\left(\frac{3-\sqrt{3}}{6}\right)}{6\arcsin\left(\frac{3-\sqrt{3}}{6}\right)}$$
$$\approx 1.459 \approx 3:2 \tag{7}$$

A ceramic system may be treated as an ensemble of domains, and each domain can be considered to be the system we have discussed above. Then, eq. (7) represents the molar ratio of the rhombohedral and tetragonal phases for a PZT ceramic of the MPB composition. This molar ratio can be calculated directly from X-ray diffraction intensities, therefore eq. (7) provides a criterion for the determination of the MPB.

Thermodynamics tells us that maximum values of many physical quantities should appear at the MPB composition due to the existence of maximum number of energetically degenerated states. However, several experimental results reveal that these maxima do not match with the MPB on Fig. 1 but often slightly deviate to the rhombohedral side.[4,5] Our analysis above gives a reasonable explanation to this controversy. Naturally, if we use the ratio of 3:2 instead of 1:1 as the criterion for

the MPB, the MPB line on Fig. 1 would shift to the rhombohedral side.

The novel idea presented in this paper is to take into account the geometrical constraints in the calculation of the statistical distributions of those energetically degenerated states in solids. Through this paper we also intend to bring people's attention on treating solid systems, those thermodynamic theories developed for gas and liquid systems may not be valid and should be augmented to incorporate the characteristics of solids.

Finally, we like to point out that a special property pertaining to this problem has been used implicitly, i.e., the homotopy mapping between the real space and the order parameter space. Strictly speaking, thermal motion occurs in real space not in order parameter space. But because the order parameter is a vector in our problem, there is a one point to one point mapping between the real space and the order parameter space, therefore we did not emphasize the difference between the two spaces in the text. However, if the order parameter is not a vector, one can not use the theory developed in this paper.

One of the authors (W.C.) wishes to thank Drs. M. Grutzeck and A. Saxena for helpful comments. This research was supported by Air Force Office of Scientific Research under Grant No. AFOSR-91-0433.

References

1) B. Jaffe, W. R. Cook and H. Jaffe: *Piezoelectric Ceramics* (Academic Press, London, 1971) p. 136.
2) V. A. Isupov: Fiz. Tver. Tela 12 (1970) 1380. Translation: Sov. Phys.-Solid State 12 (1970) 1084.
3) M. J. Haun, E. Furman, H. A. McKinstry and L. E. Cross: Ferroelectrics 99 (1989) 27.
4) W. Wersing: Ferroelectrics 7 (1974) 163.
5) K. Carl and K. H. Hardtl: Phys. Status Solidi a 8 (1971) 87.

PHYSICAL REVIEW B

CONDENSED MATTER

THIRD SERIES, VOLUME 47, NUMBER 9 1 MARCH 1993-I

Theoretical model for the morphotropic phase boundary in lead zirconate–lead titanate solid solution

Wenwu Cao and L. Eric Cross

Materials Research Laboratory, The Pennsylvania State University, University Park, Pennsylvania 16802

(Received 18 February 1992; revised manuscript received 14 September 1992)

A statistical model is proposed to address the problem of two-phase coexistence near the morphotropic phase boundary (MPB) in $Pb(Zr_{1-x}Ti_x)O_3$ solid-solution series. Functional forms for the molar fractions of tetragonal and rhombohedral phases inside the coexistence region are obtained, which may be used to replace the lever rule to describe the phase mixing in a complete binary solid-solution series without solubility gap. The model predicts that the width of this coexistence region is inversely proportional to the volume of each element in the statistical ensemble. In addition, the shift of the MPB composition from the composition of equal molar fraction of the two coexisting phases is found to be proportional to the width of the coexistence region. Several existing controversial experimental observations can be reconciled by this model.

I. INTRODUCTION

The most widely used piezoelectric ceramic today is lead zirconate titanate (PZT), a solid solution of $PbZrO_3$-$PbTiO_3$, with compositions near the morphotropic phase boundary (MPB). A MPB is defined as a compositional phase boundary at which the two adjacent phases in a phase diagram have equal Gibbs free energy. The phase diagram determined by Jaffe, Cook, and Jaffe[1] from x-ray-diffraction measurements is shown in Fig. 1. The MPB on this phase diagram was considered to be the composition at which the amount of tetragonal and rhombohedral phases is equal.[1] However, it was pointed out[2] that the molar ratio of the two low-temperature phases, i.e., rhombohedral:tetragonal, should be 3:2 instead of 1:1 at the MPB (defined by equating the free energies of the two phases), which provides an explanation for the discrepancy between the MPBs determined by using dielectric maximum and from x-ray-diffraction intensities.

Historically, the exact composition of MPB in PZT has never been precisely defined; it ranges from 45–50 mol % of $PbTiO_3$.[3–6] There is a coexistence region of the tetragonal and rhombohedral phases whose width is also not well defined,[5–9] ranging from 2–15 mol % of $PbTiO_3$ around the composition Ti/Zr=48/52.

From many years of study on the PZT system, the following two facts are well accepted:

(1) The PZT system is a complete binary solid solution of $PbTiO_3$ and $PbZrO_3$ without solubility gaps.

(2) Below the paraelectric-ferroelectric transition temperature there exists a coexistence region of the tetragonal and rhombohedral phases near the MPB composition, although the width of this region is still a debatable issue. Adding small amounts of dopant can shift the MPB and increase the width of the coexistence region.

The lever rule, obtained from mass conservation, has been used to describe fact (2) above.[7,8] Although the data

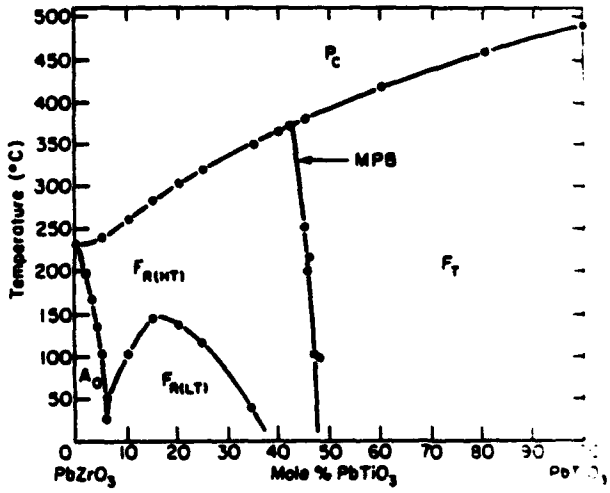

FIG. 1. Phase diagram of $PbZrO_3$-$PbTiO_3$ (PZT) solid-solution series by Jaffe, Cook, and Jaffe (Ref. 1).

fitting appears to be reasonable, the two edge compositions x_1 and x_2 in the lever rule actually specify a solubility gap, which is in contradiction with fact (1) above. An alternative explanation of the phase coexistence [fact (2) above] is to use the transition hysteresis argument within the context of a first-order phase transition by taking the composition as an independent variable.[10] This is also inadequate because the composition variable is already frozen in the temperature region ($T < 375$ °C) where the two ferroelectric phases exist; the system only experiences a diffusionless structural phase transition at the Curie point. Solid-state reaction, which is needed to change the composition of PZT, cannot occur until above 800 °C. In other words, once a solid solution is formed at high temperature ($T > 800$ °C), the chemical composition cannot be changed at low temperatures, but the system can have temperature-induced diffusionless structural phase transitions. Because the compositional degree of freedom has been frozen in the temperature region of interest, the transition hysteresis concept is not feasible. In addition, both explanations mentioned above lead to a definite width of the coexistence region which has not been observed experimentally.

Many physical properties of PZT reach their maximum or minimum at the MPB, which is also not well understood. From the definition of MPB, the two low-temperature structural phases are energetically degenerate at the MPB composition, and it is conceivable that the electric field or stress-driven phase transitions between the two ferroelectric structures are possible for the PZT of composition near the MPB. This field-induced phase transition could contribute substantially to the observed phenomena. In order to quantify this contribution, one must know the exact fraction of the two structural phases for a given composition in the low-temperature regime. Looking at classical thermodynamic and statistical theories, one finds that they cannot be directly applied to address our problem because the MPB is defined by equating the free energies of the tetragonal and rhombohedral phases, hence the energy difference (which is the only criterion in classical statistics) is zero. On the other hand, after a low-temperature structure is formed from the paraelectric-ferroelectric phase transition, the system may be "locked" into this structure because of the existence of a transition barrier between the two low-temperature phases (this is reflected in Fig. 1 as the nearly vertical line of the MPB). This "locked structure" is thermodynamically metastable below the transition temperature. Therefore, in reality we are not exactly dealing with the absolute thermodynamic equilibrium at temperatures well below T_c. It is our opinion that the coexistence of the two low-temperature phases in the PZT system is a result of quenched-in thermal fluctuations. Following this idea, the two observations in the PZT system mentioned above can be explained satisfactorily, and the fractions of the two coexisting phases can be quantified.

II. THE MODEL

As a starting point, we assume that the partitioning of the two phases does not change with temperature after being determined at the paraelectric-ferroelectric phase transition. We therefore only need to calculate the partitioning near T_c.

The question we are trying to address here is really the accessibility of all the low-temperature states during the phase transition. If we assume that all 14 states (8 in the rhombohedral phase and 6 in the tetragonal phase) are identical, then the molar ratio, rhombohedral:tetragonal, should be 4:3 at the MPB. But obviously these 14 states are not identical, the two low-temperature structures are geometrically *inequivalent*. In Ref. 2 we have applied this geometrical constraint in the statistical calculation of this ratio at the MPB, which is close to 3:2, and introduced the concept of probability polyhedron for systems with a vector order parameter. This concept may be used to calculate the distribution of energetically degenerate but geometrically inequivalent states resulting in a second-order phase transition (here the transition refers to the paraelectric-ferroelectric transition but not the one between the two low-temperature phases). In this paper we try to extend the model discussed in Ref. 2 to account for the coexistence of two energetically nondegenerate and geometrically inequivalent phases by incorporating the classical statistics.

In order to understand the underlying physics of the present problem, we first study the driving force for the phase transition. It has been shown using phenomenological theory that the paraelectric to ferroelectric phase transition in PZT for compositions in the vicinity of the MPB is of second order.[11] Therefore, thermal fluctuations are the driving force for this phase transition. Inevitably, these fluctuations will also play a key role in the probability distribution of the tetragonal and rhombohedral phases during cooling through the Curie point.

A. The probability polyhedron

The construction of probability polyhedron was described in Ref. 2. The only assumption made there was the orientational ergodicity of thermal fluctuations which is valid for either long-time observation of a single system or instant observation of a statistical ensemble.

In order to generalize the idea of probability polyhedron we give an equivalent definition below. Considering the fact that the number of surface planes in the polyhedron is equal to the number of allowed polarization directions, it is equivalent to say that in the fluctuating state each of the polarization states occupies an effective solid angle in the order parameter space, which is equal to the solid angle subtended by the polyhedron surface whose plane normal coincides with that polarization direction. The probability of attaining this polarization state on cooling through the phase transition is equal to its effective solid angle divided by 4π, the normalization constant.

Now we use this concept to describe the distribution of polarization states for the PZT of compositions sufficiently far from the MPB. In this case, the low-temperature phase is either tetragonal or rhombohedral. On the tetragonal side (Ti rich) of the MPB, the probability polyhedron is a cube with each of the six variants,

$(\pm p,0,0)$, $(0,\pm p,0)$, and $(0,0,\pm p)$, occupying an effective solid angle of $\Omega_i = 2\pi/3$ $(i=1-6)$, where p is the magnitude of the polarization. Hence, the fraction being transformed into each of the polarization states in an ensemble (a ceramic can be treated as an ensemble of grains) is equal to $\Omega_i/(4\pi)=1/6$, and the total polarization of the ensemble is zero in the order parameter space. Because of the one to one point mapping between the order parameter space and the real space, the total polarization in the real space is also zero for a statistical ensemble of particles. The same can also be said for the compositions on the rhombohedral side (Zr rich) of the MPB, for which the probability polyhedron is an octahedron. The effective solid angle for each variant is $\pi/2$ and the probability for each polarization state is $(\pi/2)/(4\pi)=1/8$. Again, the net polarization of the ensemble of rhombohedral phase particles is zero. When the PZT composition is close to the MPB composition, the two low-temperature structural phases can coexist and the probability polyhedron will have 14 faces. In general, the tetragonal states and the rhombohedral states are not degenerate unless the composition is exactly on the MPB; therefore, we expect the effective solid angle representing the probability of each polarization state to change with composition.

There is an energy difference between the two structural phases when the composition is not exactly on the MPB; we introduce an anisotropy factor δ to describe this situation. As shown in Fig. 2, the distance of the surfaces (corresponding to different phases) from the center point of the polyhedron is represented by r_i $(=\overline{OT}$ or $\overline{OR})$, which controls the solid angle subtended by the surface. In other words, r_i determines the probability of attaining a specific polarization state using the concept we have introduced above; r_i must be a function of energy. At the MPB composition, the tetragonal and the rhombohedral phases are degenerate, and we have $r_T = r_R$. In this case, the actual magnitude of r_i does not matter since the solid angle partitioning is independent of r_i. But for the nondegenerate case, r_T and r_R are different and should depend on the energies of the two low-temperature phases. We define the distribution anisotropy parameter δ as follows:

$$\delta = \frac{r_T - r_R}{r_T} , \tag{1}$$

which is a function of composition only when temperature and pressure are fixed.

$\delta=0$ represents the MPB composition, at which the probability ratio of the rhombohedral and tetragonal phases is[2]

$$\frac{f_R}{f_T} = \frac{\pi - 6\arcsin[(3-\sqrt{3})/6]}{6\arcsin[(3-\sqrt{3})/6]} , \tag{2}$$

where f_R and f_T are the probabilities of the rhombohedral and tetragonal phases. This ratio is close to 3:2 instead of 1:1 given by Jaffe, Cook, and Jaffe.[1]

B. The distribution functions for the coexisting phases in PZT of composition near the MPB

There are upper and lower bounds for the value of δ. When δ decreases, the probability of transforming into the rhombohedral phase also decreases until $\delta = 1-\sqrt{3}$; for δ less than this critical value, the low-temperature phase can only be tetragonal because the polyhedron becomes a cube. On the other hand, when δ increases, the probability of transforming into the tetragonal phase decreases, the upper limit for δ is $1-1/\sqrt{3}$, for $\delta \geq 1-1/\sqrt{3}$; the polyhedron becomes an octahedron, which means that the system can only be rhombohedral. There is another special value of δ, $\delta = 1-2/\sqrt{3}$, at which the representative surface of the rhombohedral phase on the probability polyhedron changes its shape from a six-sided polygon to a right triangle, and the representative surface for the tetragonal phase changes from a square to an eight-sided polygon. Therefore, in calculating the effective solid angle for each of the polarization states, one must use Figs. 2 and 3 for the cases of $\delta > 1-2/\sqrt{3}$ and $\delta < 1-2/\sqrt{3}$, respectively. It can be

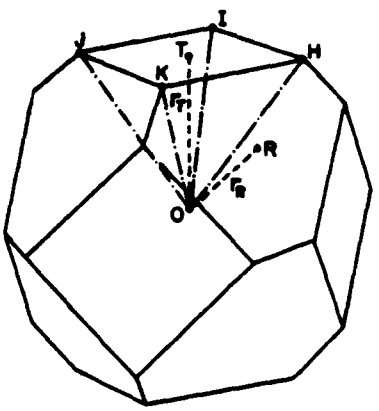

FIG. 2. Probability polyhedron for PZT system with the parameter δ in the range $1-1/\sqrt{3} > \delta > 1-2/\sqrt{3}$. At MPB, $\overline{OT} = \overline{OR}$ and $\delta = 0$.

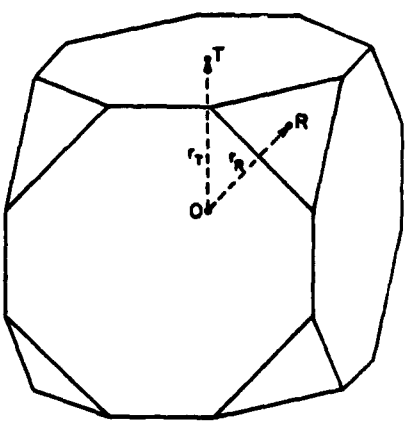

FIG. 3. Probability polyhedron for PZT system with the parameter δ in the range $1-2/\sqrt{3} > \delta > 1-\sqrt{3}$, $r_T \neq r_R$.

shown that[12]

$$f_T=\begin{cases}\dfrac{6}{\pi}\arcsin\left[\dfrac{\sqrt{3}[2(1-\delta)-\sqrt{3}]}{2(1-\delta)^2+[\sqrt{3}-(1-\delta)]^2}\right], & 1-\sqrt{3}<\delta<1-\dfrac{2}{\sqrt{3}}\ ;\\ \dfrac{6}{\pi}\arcsin\left[\dfrac{[\sqrt{3}(1-\delta)-1]^2}{2+[\sqrt{3}(1-\delta)-1]^2}\right], & 1-\dfrac{2}{\sqrt{3}}<\delta<1-\dfrac{1}{\sqrt{3}}\ .\end{cases} \tag{3}$$

$$f_R=1-f_T\ . \tag{4}$$

C. The physical meaning of δ and the width of the coexistence region

In the PZT system, the free energies of the tetragonal and rhombohedral phases, G_T and G_R, depend monotonically on composition. The two free energies cross each other at the MPB.[13] From thermodynamics, at equilibrium only one of the two low-temperature phases is stable except at the MPB composition. However, in the vicinity of the MPB, one expects the energy difference of the two low-temperature phases to be very small; thermal energy can introduce some uncertainties in the distribution f_i, which obeys the canonical distribution. Since we have assigned the solid angle Ω_i to be proportional to the distribution function f_i, Ω_i may be written as follows:

$$\Omega_i\propto f_i\propto\exp\left[-\frac{G_i-G_c}{kT_c}\right], \tag{5}$$

where k is Boltzmann's constant, G_i and G_c are the system free energies for the ith low-temperature structural phase and for the lowest energy phase ("ground state"), respectively. For a given surface area, the solid angle it subtends with respect to a given point in space is inversely proportional to the square of the distance between the surface and that point, i.e., $\Omega_i\propto 1/r_i^2$. Hence, from Eq. (5) the distance variable r_i can be written in terms of the free-energy difference:

$$r_i\propto\frac{1}{\sqrt{\Omega_i}}=\exp\left[\frac{G_i-G_c}{2kT_c}\right]. \tag{6}$$

By substituting Eq. (6) into Eq. (1) the parameter δ becomes

$$\delta=1-\exp\left[\frac{G_R-G_T}{2kT_c}\right]. \tag{7}$$

Using Eq. (7) and the limiting values of δ, one can calculate the required energy difference in order to obtain a single phase state:

$$|G_R-G_T|>kT_c\ln 3\ . \tag{8}$$

Therefore, the width of the coexistence region depends on how fast the energy difference G_T-G_R changes with composition. An important conclusion can be drawn from Eq. (8); the width of the MPB depends on the volume of the element in the ensemble (for example, the particle size in a powder system). This is because the free-energy difference on the left-hand side of Eq. (8) is an extensive variable while the product on the right-hand side is an intensive variable. This point can become more transparent if we recast Eq. (8) in the following form:

$$|g_R-g_T|=\frac{kT_c}{v}\ln 3\ , \tag{9}$$

where g_T and g_R are the free-energy densities of the two phases and v denotes the volume of each element in the statistical ensemble. Because the free-energy difference is small for PZT compositions sufficiently close to the MPB, we may write the free-energy density difference in terms of a series expansion around the MPB composition:

$$g_R-g_T=\sum_{n=1}^{\infty}\alpha_n(x-x_0)^n\ , \tag{10}$$

where x is the composition variable and x_0 is the MPB composition, and

$$\alpha_n=\frac{\partial^n}{\partial x^n}(g_R-g_T)|_{T,P}\ . \tag{11}$$

Note that Eq. (10) is a mathematical representation but not the Landau free energy, and there are no symmetry constraints for the expansion coefficients.

In a linear approximation, i.e., taking $\alpha_n=0$ for $n\neq 1$, the width of MPB δx can be derived using Eqs. (9) and (10):

$$\Delta x=\frac{2kT_c}{\alpha_1 v}\ln 3\ . \tag{12}$$

Equation (12) indicates to us that the width of the coexistence region, Δx, is inversely proportional to the volume of the statistical element. Suppose Δx is 0.1 for a particle size of 0.1 μm, then it would be 0.0125 for a particle size of 0.2 μm. Therefore, it is not surprising that the values of Δx obtained by different processing techniques are quite different. It is also conceivable that for a well-sintered ceramic system or a single-crystal system, Δx will be too small to be detectable with the available experimental techniques, which gives an explanation as to why the coexistence could not be observed in some experiments, especially in a single-crystal system.

III. COMPARISON WITH EXPERIMENTS

Using the linear approximation, we can rewrite Eq. (7) in the following form:

$$\delta = 1 - \exp\left[\frac{(x - x_0)\ln 3}{\Delta x}\right] . \tag{13}$$

Here x_0 is the MPB composition and Δx is the width of the coexistence region as mentioned above. These two parameters can be obtained from fitting experimental data to the distribution functions given by Eqs. (3) and (4). In practice, the molar ratio of the two coexisting phases is measured from the integrated intensities of the x-ray-diffraction peaks of the rhombohedral and tetragonal phases. The value of x_0 may be obtained using Eq. (2), viz., at $x = x_0$ the intensity ratio of the rhombohedral phase to the tetragonal phase is roughly 3:2. Because the x-ray technique has a limited accuracy for a second phase of less than a few percent, especially when the diffraction peaks are not well separated, it is difficult to measure the coexistence width Δx. In order to overcome this difficulty, a useful relation is given below:

$$x_m - x_0 = \Delta x \left\{ \frac{1}{\ln 3} \ln \left[1 + \left[\frac{2\sin(\pi/12)}{1-\sin(\pi/12)} \right]^{1/2} \right] - \frac{1}{2} \right\}$$

$$\approx 0.053 \Delta x , \tag{14}$$

where x_m is the equal fraction composition at which the molar ratio of the two phases is 1:1, which can be easily obtained from x-ray-diffraction measurements. Equation (14) was obtained by substituting Eq. (13) into Eq. (3) and letting $f_T = 1/2$.

For the pure PZT system, the coexistence region is not only very narrow but also very sensitive to the processing procedures; there are no reliable diffraction data in the literature. But when the system is slightly doped, the coexistence region becomes wider and the peaks become easily identifiable. As an example, we examine the experimental data of Hanh, Uchino, and Nomura,[8] which is for the solid-solution system

$$0.1Pb_{0.9}K_{0.1}(Zn_{1/3}Nb_{2/3})O_{2.95} - (0.9-x)PbZrO_3 - x\,PbTiO_3 .$$

The squares and circles in Fig. 4 are the measured molar fractions of the rhombohedral and the tetragonal phases, respectively; the solid curves were obtained by Hanh, Uchino, and Nomura from fitting the experimental data to the lever rule, and the dotted curves are from the current model. Linear approximation [Eq. (13)] was used in the calculation and the two parameters $x_0 = 0.5027$ and $\Delta x = 0.2066$ were fitted to the experimental data using the nonlinear Levenberg-Marguardt method. The two special compositions x_0 (MPB) and x_m are also given in Fig. 4 as references.

Generally speaking, linear approximation is valid only when the two free-energy curves are relatively straight as a function of composition near the crossover point of the two free energies. It is expected that the calculated coexistence region could become slightly narrower when the full expansion in Eq. (10) is used.

From Fig. 4 one may find that the lever rule seems to give a good fit to the limited experimental data points, however, the derivatives of the distributions, df_R/dx and df_T/dx are discontinuous at the compositions x_1 and x_2, which represent the existence of a solubility gap between x_1 and x_2. This is in contradiction with the complete solubility of the system. On the other hand, our model not only provides excellent fit to the experimental data, but also eliminates such derivative discontinuities, which makes it more suitable for describing the phase mixing in complete solid-solution systems.

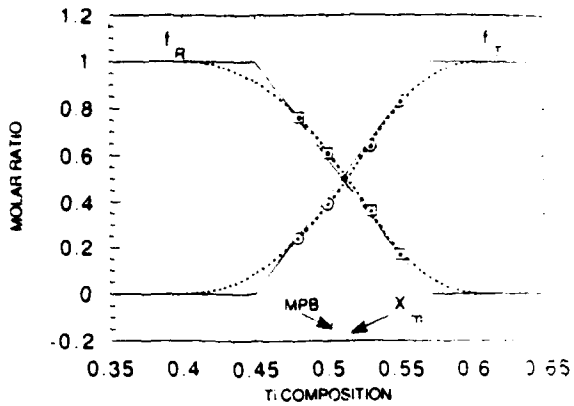

FIG. 4. The molar fractions of the rhombohedral and tetragonal phases inside the coexistence compositional region for $0.1Pb_{0.9}K_{0.1}(Zn_{1/3}Nb_{2/3})O_{2.95} - (0.9-x)PbZrO_3 - x\,PbTiO_3$ solid solution. The squares and circles are the experimental data from Ref. 8, the solid curves were fitted from the lever rule, and the dotted curves were calculated using the proposed model under linear approximation.

In order to further illustrate the difference between the two theories, let us look at a binary system AC-BC and assume they form solid-solutions α and β for A-rich and B-rich compounds, respectively. Then, for any given composition x inside the coexistence region of α and β, we have the two theories describe the following situations:

(a) Lever rule

$$xAC + (1-x)BC = f_\alpha A_{x_1}B_{1-x_1}C(\alpha \text{ structure}) + f_\beta A_{x_2}B_{1-x_2}C(\beta \text{ structure}) ; \tag{15}$$

(b) Present model

$$xAC + (1-x)BC = f_\alpha A_x B_{1-x} C(\alpha \text{ structure}) + f_\beta A_x B_{1-x} C(\beta \text{ structure}) . \tag{16}$$

The lever rule specifies a solubility gap from x_1 to x_2, and the two coexisting phases have different chemical compositions as shown on the RHS of Eq. (15). On the other hand, our model was derived from the complete solubility of AC and BC, indicated on the RHS of Eq. (16), and the phase coexistence was considered as a frozen-in second metastable phase from thermal fluctuations.

IV. SUMMARY AND CONCLUSIONS

A theoretical treatment is proposed to calculate the molar fractions of the rhombohedral and tetragonal

phases near the MPB in a PZT system. Under the assumption that the partitioning of the two low-temperature phases is determined at the paraelectric-ferroelectric transition, the distribution functions are related to the effective solid angles associated with the low-temperature phases in the order parameter space. Analytic forms were obtained for the molar fractions of the two low-temperature phases inside the coexistence region. These molar fractions depend on a single parameter δ, which is a function of the free-energy difference of the two low-temperature phases. Besides the energy considerations, the geometrical constraints of a solid structure have been incorporated in the statistical calculations.

Using this model, the two contradictory facts of the PZT system mentioned in the introduction can be reconciled, as the current model allows for the phase coexistence in a complete solid-solution system without solubility gaps. In addition, the controversy about the undefined width of the coexistence region may also be explained using Eq. (9), which states that the width of the coexistence region is inversely proportional to the volume of the element in a statistical ensemble (such as the particle size in a powder system). Because the particle (or grain) size depends strongly on the processing technique, a unique value for the width Δx cannot be well defined. The coexistence should not occur in a single-crystal system, which is consistent with the experimental observations.

The model was applied to the experimental data of Hanh, Uchino, and Nomura,[8] which is for the complete solid-solution system, $0.1Pb_{0.9}K_{0.1}(Zn_{1/3}Nb_{2/3})O_{2.95}-(0.9-x)PbZrO_3-xPbTiO_3$, and compared with the fitting using the lever rule. Although both theories provide good fit to the experimental data, the solubility gap specified by the lever rule makes it unsuitable to this problem, while the current proposed treatment can eliminate the two unphysical kinks in the distribution functions at x_1 and x_2 given by the lever rule. Therefore the proposed model is more consistent with the nature of complete solid-solution systems. Several predictions were made from the current model, including the relationship between the width Δx and the particle volume, which await further experimental verifications.

ACKNOWLEDGMENT

This research was supported by Air Force Office of Scientific Research under Grant No. AFOSR-91-0433.

[1]B. Jaffe, W. R. Cook, and H. Jaffe, *Piezoelectric Ceramics* (Academic, London, 1971), p. 136.

[2]W. Cao and L. E. Cross, Jpn. J. Appl. Phys. **31**, 1399 (1992).

[3]E. Sawguchi, J. Phys. Soc. Jpn. **8**, 615 (1953).

[4]B. Jaffe, R. S. Roth, and S. Margullo, J. Res. Nat. Bur. Stand. **55**, 239 (1955).

[5]A. V. Turik, M. F. Kupriyamov, E. N. Sidorenk, and S. M. Zaitsev, Zh. Tekh. Fiz. **50**, 2146 (1980) [Sov. Phys. Tech. Phys. **25**, 1251 (1980)].

[6]P. Gr Lucuta, F. L. Constantinesan, and D. Barb, J. Am. Ceram. Soc. **68**, 533 (1985).

[7]P. Ari-Gur and L. Benguigui, Solid State Commun. **15**, 1077 (1978).

[8]Lu Hanh, K. Uchino, and S. Nomura, Jpn. J. Appl. Phys. **17**, 637 (1978).

[9]M. L. A. Dass, U. Dahmen, G. Thomas, T. Yamamoto, and K. Okazaki, in *Proceedings of The Sixth IEEE International Symposium on Applicatio of Ferroelectrics, Bethlehem, PA,* edited by W. A. Smith (IEEE, New York, 1986), p. 146.

[10]V. A. Isupov, Fizika Tverd. Tela (Leningrad) **12**, 1380 (1970) [Sov. Phys. Solid State **12**, 1084 (1970)].

[11]M. J. Haun, E. Furman, H. A. McKinstry, and L. E. Cross, Ferroelectrics **99**, 27 (1989).

[12]W. Cao and L. E. Cross, J. Appl. Phys. (to be published).

[13]M. J. Haun, E. Furman, S. J. Jiang, and L. E. Cross, Ferroelectrics **99**, 63 (1989).

A Transmission Electron Microscopy Investigation of the R3m → R3c Phase Transition in $Pb(Zr,Ti)O_3$ Ceramics

C.A. Randall, M. Matsko, W. Cao, and A.S. Bhalla
Materials Research Laboratory
The Pennsylvania State University
University Park, PA 16802

Abstract

A transmission electron microscopy (TEM) study was performed on $Pb(Zr,Ti)O_3$ compositions within the R3m → R3c phase region. The low temperature phase is owing to a displacive phase transition involving oxygen octahedral tilts. The associated superlattice reflections are detectable by electron diffraction. Dark Field diffraction contrast imaging of the superlattice reflections reveals antiphase boundaries associated with octahedral tilt domains. Interaction between the octahedral tilt antiphase boundaries and the ferroelectric domain structures of the R3c phase is studied and discussed .

Introduction

The perovskite solid-solution between end-member $PbTiO_3$ and $PbZrO_3$ is the basis of important technological ceramics used in piezoelectric, pyroelectric and electro-optic applications.[1,3] The phase diagram of $PbZrO_3$-$PbTiO_3$ is illustrated in Figure 1. The phase diagram contains a variety of displacive phase transitions and there are antiferroelectric and various ferroelectric phases in the low temperature regime. Compositions between Zr/Ti ratios 90/10 and 65/35 reveals a ferroelectric → ferroelectric transition between rhombohedral space groups R3m → R3c. This transition involves the oxygen octahedra tilt about the <111> directions.[4] The aim of this investigation is to study the inter-relationship between octahedral tilt domain structures and the high temperature ferroelectric domain structures. There have been virtually no studies regarding the domain structures of octahedral tilt systems in perovskites.[5] The transmission electron microscope offers an attractive means to study this subtle phenomena owing to electron scattering factors being much larger than x-ray scattering factors. The diffraction contrast imaging also allows a direct means to study the domain states.[6]

Experimental

Ceramic samples of $Pb(Zr,Ti)O_3$ were made using conventional solid-state sintering techniques. The starting raw material powders were of analytical grade quality and included PbO, ZrO_2, and TiO_2. Two compositions were made for this study $Pb(Zr_{0.9}Ti_{0.1})O_3$ and $Pb(Zr_{0.65}Ti_{0.35})O_3$. These compositions were batched according to stoichiometric ratios and accounting for loss of ignitions. The raw powders were ball milled with ethanol solvent for 48 hours for complete mixing. Perovskite phases were fully formed after calcining for four hours at 900°C, as determined by a Scintag X-ray diffractometer. The calcined powder was ball milled for 24 hours. Binder and 1 wt% excess PbO was added to 80 mesh sieved powders. Green pellets with 60% theoretical density were formed using uniaxial pressure followed by binder burnout at 550°C for 1 hour. Sintering was undertaken at 1250°C for 2 hours to give pellets from 91-94% theoretical density and less than 1 percent weight loss.

TEM samples were [redacted] to a thickness ≈ 50 μm. These sections were mounted [redacted] minute epoxy. Ion beam thinning was performed at [redacted] a beam current ~ 1 mA. TEM observations were made using a Philips 420 STEM at 100 k.v. A Gatan liquid nitrogen two-tilt stage was used to make in situ TEM observations between 80°C to -180°C.

Results

Figures 2 (a) and (b) show the [110] zone axis diffraction patterns revealing {h + 1/2, k + 1/2, l + 1/2} pseudo cubic superlattice reflections in $Pb(Zr_{0.9}Ti_{0.1})O_3$ and $Pb(Zr_{0.65}Ti_{0.35})O_3$ respectively. It is found that by heating the $Pb(Zr_{0.65}Ti_{0.35})O_3$ sample to 80°C the superlattice reflection disappears, Figure 2(a), and conversely cooling to lower temperatures with the Gatan liquid nitrogen stage the intensity increases. These reflections are, therefore, associated with a displacive phase transition. The {h + 1/2, k + 1/2, l + 1/2} diffractions are consistent with the neutron diffraction study performed by Glazer.[4] Glazer predicted the origin of this superstructure to be oxygen octahedral tilts within the simple perovskite structure. The oxygen octahedral shifts with equal components about the pseudo-cubic perovskite axis as to give an effective clockwise and anticlockwise rotation of oxygen octahedra about the <111> directions parallel to the ferroelectric dipole displacements of the R3m phase, Figure 3.

Figure 4(a) shows the dark field diffraction contrast image associated with the superlattice reflection in a $Pb(Zr_{0.9}Ti_{0.1})O_3$ subgrain. A dark ribbon-like boundary is observed under these

imaging conditions, and this is believed to be a wall separating out-of-phase octahedral tilt variants. Figure 4(b) shows the same subgrain imaged under a multiple beam bright field condition. This reveals 180° domain boundaries within this region. There is only a weak spatial perturbation between the 180° ferroelectric domain walls and the octahedral antiphase boundaries.

Figure 5(a) shows a bright field image which reveals ferroelectric twin structures and inversion 180° ferroelectric domains typical in a rhombohedral ferroelectrics.[5] Figure 5(b) shows the same crystallite imaged in dark field with a superlattice reflection. The antiphase boundary contrast is again observed and shows a strong interaction with the twin boundaries. Generally we found antiphase boundaries are terminated on the twin boundaries, grain boundaries, or alternatively contained within closed loops. The antiphase boundaries in the $Pb(Zr,Ti)O_3$ ceramics predominantly terminate on either twin boundaries or grain boundaries. Region X in Figure 5(b) shows an example of the antiphase boundary terminated at a {110} twin domain boundary region Y shows an antiphase boundary to be coincident with a {001} domain wall.

Discussion

From the above results we can infer that the R3m ferroelectric phase has only twin and inversion domains. Twin domains being 109° or 71° type and twin on habit planes {110} and {100}, respectively. These observations are consistent with earlier observations on modified rhombohedral $Pb(Zr,Ti)O_3$ ceramics.[7] The octahedral tilt transition is driven by a zone boundary soft mode resulting in the doubling of the unit cell. The reflections observed are consistent with the proposed model by Glazer, Figure 3. This transition gives rise to two additional variants which are separate from each other with antiphase boundaries. The antiphase boundaries are slightly perturbed by 180° domain walls and are strongly perturbed by the twin boundaries. In some incidents we noted that the anti-phase boundaries were consistent with the twin walls which may imply a coupling between the gradients of the tilt and the polarization.

Acknowledgements

This research was supported by Air Force Office of Scientific Research under Grant No. AFOSR-91-0433 and by Office of Naval Research under Grant No. N00014-92-J-1510. We also wish to thank Ian Reany for many discussions during his work.

Figure Captions

Figure 1. The $PbZrO_3$-$PbTiO_3$ Phase Diagram [Jaffe, Cook, Jaffe (1971)].

Figure 2. [110] Zone Axis Diffraction Patterns (a) $Pb(Zr_{0.9}Ti_{0.1})O_3$ and (b) $Pb(Zr_{0.65}Ti_{0.35})O_3$, both at room temperature, and (c) $Pb(Zr_{0.65}Ti_{0.35})O_3$ at 80°C.

Figure 3. Schematic representation of the oxygen octahedral-tilting in R3c phase.

Figure 4 (a) Dark field image of octahedral-tilt superlattice reflection revealing anti-phase boundaries (APB); (b) multiple bright field image of same area revealing typical 180° domain wall contrast.

Figure 5. (a) Dark field image of ferroelectric domain walls; (b) Dark field image of superlattice reflection revealing interaction of APBs with twin domain walls.

References

1. B. Jaffe,W.R. Cooke, and H. Jaffe, Piezoelectric Ceramics Academic Press, London, New York (1971).

2. M.E. Lines and A.M. Glass, "Principles and Applications of Ferroelectrics and Related Methods," Clarendon Press, Oxford.

3. A. Moulson and S. Herbert, "Electroceramics-Materials-Properties-Applications," Chapman and Hall, London, New York, Tokyo, Melbourne, Madras.

4. A.M. Glazer, Acta Cryst. A31, 756-762 (1975).

5. I.M. Reany, Private Communication.

6. P.B. Hirsch, A. Howie, R.B. Nicholson, D.W. Pashley, and M.J. Whelan, "Electron Microscopy of Thin Crystals," Butterworth, London.

7. C.A. Randall, D.S. Barber, and R.W. Whatmore, J. Mat. Sci. 22 935 (1987).

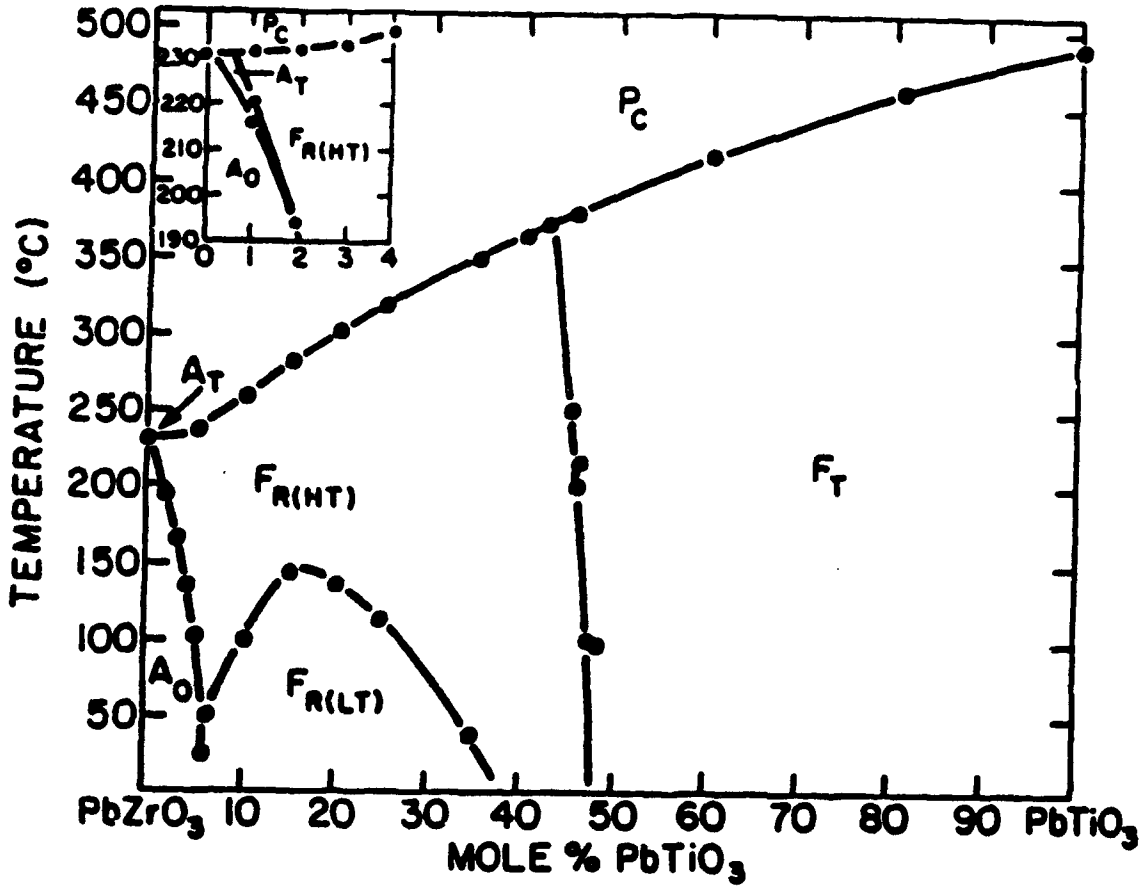

Figure 1. The $PbZrO_3$-$PbTiO_3$ Phase Diagram [Jaffe, Cook, Jaffe (1971)].

Figure 1.

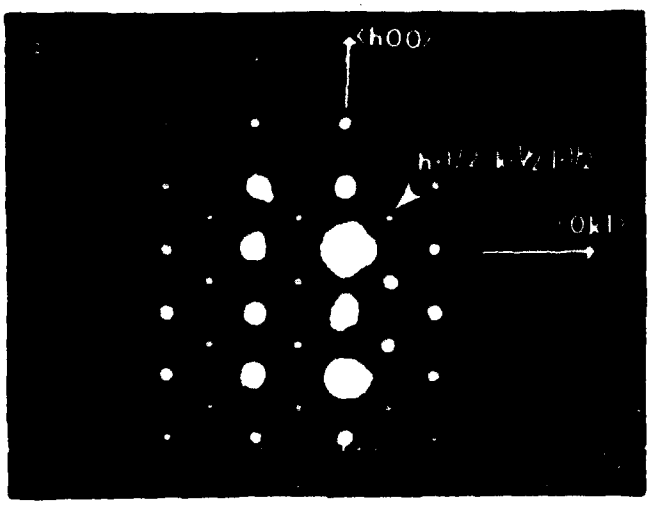

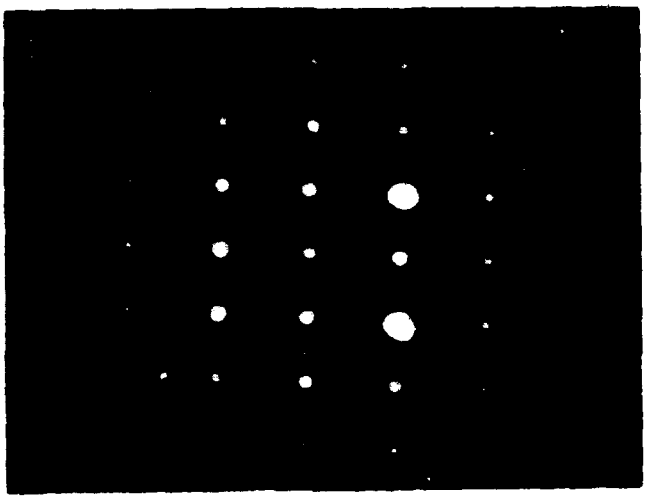

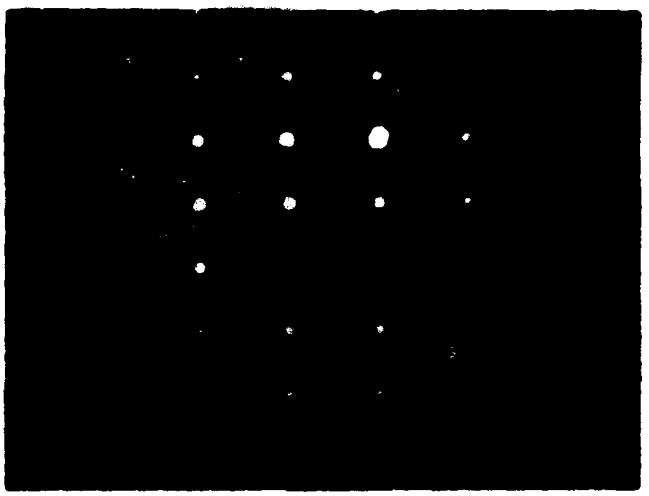

Figure 2. **[110] Zone Axis Diffraction Patterns (a) $Pb(Zr_{0.9}Ti_{0.1})O_3$ and (b) $Pb(Zr_{0.65}Ti_{0.35})O_3$, both at room temperature, and (c) $Pb(Zr_{0.65}Ti_{0.35})O_3$ at 80°C.**

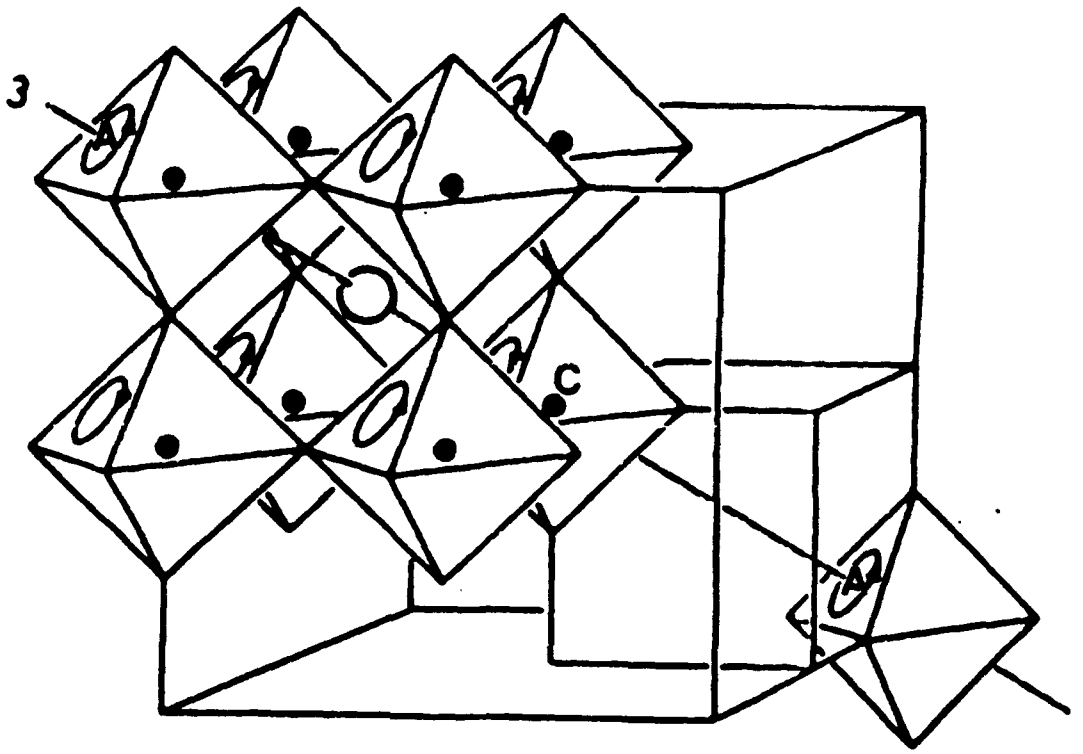

Figure 3. Schematic representation of the oxygen octahedral-tilting in R3c phase.

Figure 4 (a) Dark field image of octahedral-tilt superlattice reflection revealing anti-phase boundaries (APB); (b) multiple bright field image of same area revealing typical 180° domain wall contrast.

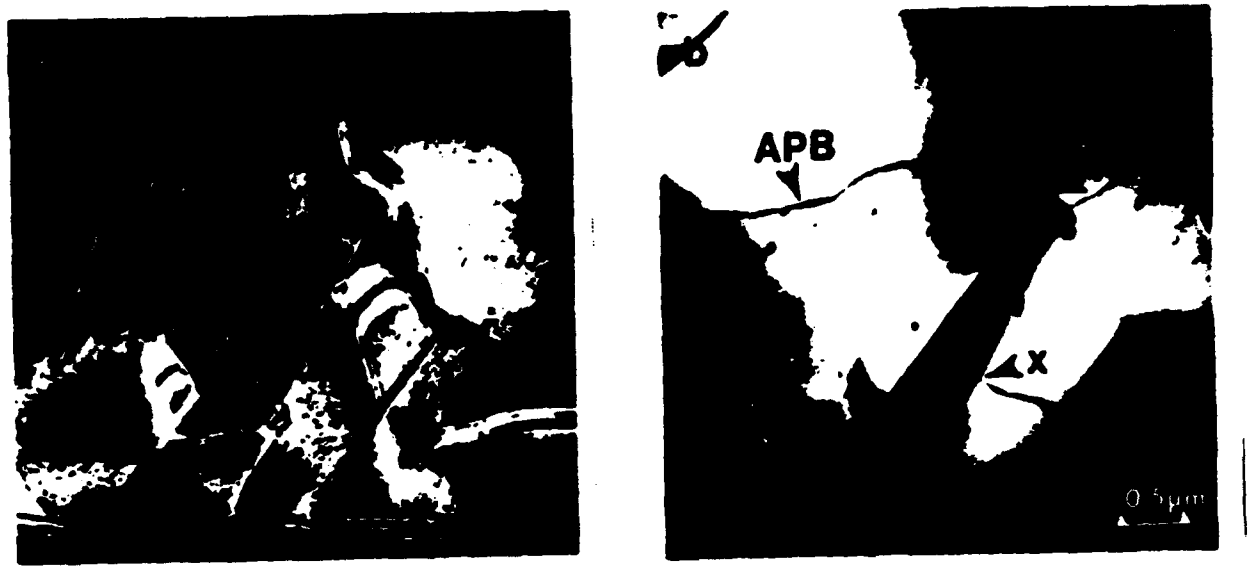

Figure 5. (a) Dark field image of ferroelectric domain walls; (b) Dark field image of superlattice reflection revealing interaction of APBs with twin domain walls.